Electrochimica Acta
Volume 229, 1 March 2017, Pages 102-111

Copper-modified titanium phosphate nanoparticles as electrocatalyst for glucose detection

Daniel Martín-Yerga [a], Javier Carrasco-Rodríguez [b], José Luis G. Fierro [c], Francisco Javier García Alonso [b], Agustín Costa-García [a]

https://doi.org/10.1016/j.electacta.2017.01.143

Copper-modified titanium phosphate nanoparticles as electrocatalyst for glucose detection

Daniel Martín-Yerga[1], *Javier Carrasco-Rodríguez*[2], *José Luis G. Fierro*[3], *Francisco Javier García Alonso*[2] *and Agustín Costa-García*[1]*

[1]Departamento de Química Física y Analítica, Universidad de Oviedo, Oviedo, Spain

[2]Departamento de Química Orgánica e Inorgánica, Universidad de Oviedo, Oviedo, Spain

[3]Instituto de Catálisis y Petroleoquímica, CSIC, Cantoblanco, 28049 Madrid, Spain

* Corresponding author: Agustín Costa-García

Departamento de Química Física y Analítica

Universidad de Oviedo

Julián Clavería 8, 330006 Oviedo, Spain

E-mail: costa@uniovi.es

Telephone: (+34) 985103488

GRAPHICAL ABSTRACT

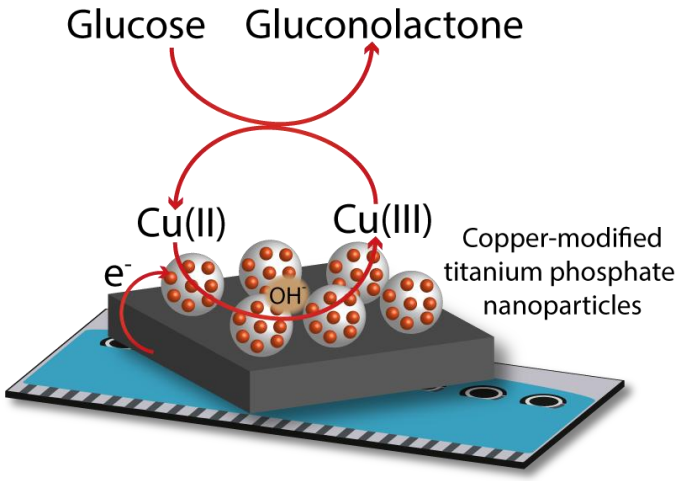

ABSTRACT

The non-enzymatic determination of glucose is a current trend in analytical chemistry. Copper-based nanomaterials are being widely employed for the fabrication of electrochemical analytical devices for glucose monitoring. In this work, copper-modified titanium phoshate nanoparticles (CuTiPNPs) were synthesized for the first time. Interestingly, CuTiPNPs show an electrocatalytic effect towards the oxidation of glucose. These nanoparticles were characterized by different techniques such as transmission electron microscopy, X-ray photoelectron spectroscopy, X-ray diffraction, infrared spectroscopy, voltammetry and electrochemical impedance spectroscopy. Important information on the structural, morphological, surface and electrochemical properties was obtained. A mechanism involving a Cu(III) species stabilized by phosphate groups of the nanoparticles is proposed for the oxidation of glucose. The analytical performance of 8-channel screen-printed electrodes modified with CuTiPNPs for glucose determination was evaluated. A wide linear range from 25 µM to 2 mM and a limit of detection of 7 µM was obtained. The good analytical figures of merit and the good selectivity towards glucose led to the versatile and accurate non-enzymatic glucose determination in real samples such as honey and plasma.

KEYWORDS: Titanium phosphate nanoparticles; Copper nanoparticles; Glucose; Electrocatalysis; Screen-printed electrodes

1. INTRODUCTION

Enzymatic electrochemical biosensors have been extensively studied and used in numerous applications due to their high selectivity and sensitivity. For instance, enzymatic sensors for the determination of alcohol[1], fructose[2], or hydrogen peroxide[3] have been developed. Glucose determination is the most widespread application of these sensors for their good performance and usefulness to monitor patients with diabetes[4,5]. However, enzymatic sensors suffer from some problems such as high price or low stability. In order to minimize these issues, a current trend is the development of non-enzymatic analytical devices for the determination of several substances of interest[6,7], and especially, glucose[8–10]. For non-enzymatic glucose detection, metallic and nonmetallic-based electrodes have been previously employed. For instance, Pissinis *et al.* have recently reported the use of a nickel-chromium alloy electrode for carbohydrates detection[11] or Tian *et al.* have reported a nickel ion implanted-modified indium tin oxide electrode for glucose determination[12]. Non-enzymatic analytical devices also present different problems such as a lower selectivity than enzymatic ones and the high price of some noble metals employed. For these reasons, solving these issues is a constant concern in order to get an ideal device for non-enzymatic glucose determination.

In recent years, nanomaterials have been widely used for different electroanalytical applications[13] such as non-enzymatic glucose detection[14]. Some nanomaterials such as metallic nanostructures, carbon nanotubes or graphene have shown great catalytic effects to electrochemical reactions. Metal nanostructures (spheres, rods, cones or cubes) can be prepared from different materials, specifically gold, platinum or palladium, as they have interesting properties in catalysis and low chemical reactivity. However, the synthesis of these nanomaterials is usually high-priced for the expensive starting materials (gold, platinum or palladium salts). The development of novel nanomaterials with similar catalytic properties to those of the noble metals but with a lower manufacturing cost is being extensively researched. Copper nanomaterials are one example. This kind of nanomaterials have

applications in fields like catalysis or analytical detectors[15,16]. For instance, glucose non-enzymatic electrochemical detection has been reported using different kinds of copper or copper oxide-modified electrodes[17–19]. The most accepted mechanism for the catalytic oxidation of sugars is the oxidation of the copper-based electrode by applying a positive potential, which, in an alkaline medium, generates Cu(III) species that react rapidly with carbohydrates [20,21]. Cu(III) species are generated only under certain conditions where they are strongly stabilized[22,23]. As stated by Baldwin *et al*.[21], although the different copper-based electrochemical devices reported are different in nature, the carbohydrate oxidation occurs only in a highly alkaline medium, and the electrode surface is basically in form of oxide or hydroxide, and the oxidation of glucose follows the same mechanism at the different electrodes. The mechanism proposed in several studies published in the literature is as follows:

$$CuO + OH^- \rightleftharpoons CuO(OH) + e^- \quad \textbf{(1)}$$

$$CuO(OH) + Glucose \rightarrow CuO + Gluconolactone \quad \textbf{(2)}$$

This mechanism involves the presence of CuO, which is oxidized to CuO(OH) after the application of a positive potential in an environment with high concentration of OH^-[20]. The Cu(III) species, which cause the carbohydrate oxidation, are electrogenerated in a stabilized atmosphere by the oxide and hydroxide groups. In all these cases, the presence of CuO seems critical to achieve the catalytic reaction.

Titanium phosphate nanoparticles (TiPNPs) have been recently developed[24]. TiPNPs, consisting in a core of crystalline $NaTi_2(PO_4)_3$ and a shell of amorphous titanium hydrogenphosphate and dihydrogenphosphate,[24] have shown to be able to interchange their acid protons by metal cations, and therefore to introduce a high amount of metals in its pore structure. These properties make them particularly suitable for the removal of heavy metals in polluted environments[25]. Another application with great potential is as label for electrochemical sensors after the introduction of a

metal easily measured by voltammetry. The ability to introduce different metals allows the use in multiplexing biosensing[26–28]. Recently, it was found that these metal-modified nanoparticles could show indirect electrocatalytic effects[29] after the *in situ* reduction of the metal to generate metallic nanoparticles on the electrode surface. For instance, silver-modified TiPNPs showed a catalytic effect towards the hydrogen evolution reaction, which could be used for quantification of these nanoparticles or as a detection method for biosensors, as it has been the case for other nanoparticles with electrocatalytic properties[30]. However, the direct electrocatalysis of reactions with TiPNPs has not been reported to date. So far, just a few metals have been introduced into the TiPNPs structure such as Cd, Pb or Ag, used for the mentioned applications, although, the introduction of other metals may prove useful for new applications.

Screen-printed electrodes are one of the most used platforms for the development of electrochemical sensors and biosensors. Their low cost, miniaturization, robustness and disposable character are valuable properties for sensing applications. It is worth noting the versatility of screen-printed electrodes to be modified either by adsorption or by covalent bonds with different materials. The disposable character eliminates the issues associated to cleaning the working electrode after performing a measurement, issues typically found with conventional electrodes. Glucose detection using screen-printed electrodes have been carried out following different approaches such as the direct electrochemistry of glucose oxidase[31], an Os-complex mediator in a Flow Injection Analysis system[32], or a gold-nanodendrite electrode[33]. On the other hand, the development of screen-printed devices continues to evolve with current trends, being the simultaneous analysis of several samples using multichannel devices one of its latest hits, which allows a considerable saving of time. As biosensing applications are time consuming, 8-channel screen-printed cards have been employed for the development of electrochemical biosensors[34–36] with other great advantages such as the low reagent consumption. Similar to ELISA plates but integrating electrochemical

detection, 96-channel screen-printed cards is a new alternative to further decrease analysis time being able to measure several samples simultaneously[37].

In this paper, a simple method to synthesize and functionalize titanium phosphate nanoparticles with copper (CuTiPNPs) and their application for non-enzymatic glucose detection using multichannel screen-printed electrodes is described. CuTiPNPs were characterized using different microscopic, structural and electrochemical techniques, obtaining relevant information about its structure and behaviour. CuTiPNPs showed a great electrocatalytic effect towards the glucose oxidation, achieving the detection of low glucose concentrations with a miniaturized and disposable device able to measure 8 samples simultaneously. The developed analytical device performed well in real samples applications.

2. MATERIALS AND METHODS

2.1. Instrumentation

Voltammetric measurements were performed with a μStat 8000 (DropSens, Spain) potentiostat interfaced to a Pentium 4 2.4 GHz computer system and controlled by DropView 8400 2.0 software. All measurements were carried out at room temperature. 8-channel screen-printed electrochemical cards (8xSPCEs) were purchased from DropSens (Spain). Each array is formed by eight 3-electrode electrochemical cells (25 μL volume) with carbon-based working and counter electrodes, whereas quasireference electrodes and electric contacts are made of silver (**Figure S1**). All the indicated potentials are related to the silver quasireference electrode. This device has dimensions of 4.0 x 7.9 x 0.06 cm (length x width x height) and the diameter of the working electrodes is 2.56 mm (geometric area of 5.14 mm^2). The 8-channel arrays were connected to the potentiostat through a specific connector, DRP-CAST1X8. An Elmasonic P ultrasonic bath (Elma GmbG, Germany) was also employed to disperse the nanoparticles in the solution.

The high resolution transmission electron micrographs (HRTEM) were obtained on a JEOL JEM 2100 transmission electron microscope with an accelerating voltage of 200 kV. X-ray diffraction (XRD) patterns were performed with a Bruker D8 X-ray diffractometer with a Cu Kα X-ray source, λ= 0.15418 nm. Fourier transform infrared (FTIR) spectroscopic measurements were taken on a Perkin Elmer FT Paragon 1000 using KBr pressed disks.

2.2. Reagents and solutions

Sulfuric acid (97%), dried ethanol, sodium hydroxide, potassium chloride and glucose were purchased from Merck (Spain). Phosphoric acid (H_3PO_4, crystalline), docusate sodium salt (AOT), titanium(IV) butoxide (TBOT), copper(II) acetate, xylose, fructose, sacarose, hexaammineruthenium(III) chloride, hexaammineruthenium(II) chloride, potassium ferrocyanide, potassium ferricyanide, dopamine hydrochloride, ascorbic acid and uric acid were purchased from Sigma-Aldrich (Spain). Diethylether and absolute ethanol were purchased from VWR. Ultrapure water obtained with a Millipore Direct Q5™ purification system from Millipore Ibérica S.A. (Madrid, Spain) was used throughout this work. All other reagents were of analytical grade. Working solutions of TiPNPs and CuTiPNPs were made in ultrapure water, and sonication was used to get disperse solutions.

2.3. Synthesis of titanium phosphate nanoparticles

Synthesis of titanium phosphate nanoparticles was carried out following a procedure found in the literature[24]. Typically, 5.65 mmol of AOT was dissolved into 12.5 g of ethanol and H_3PO_4 (51 mmol) was added. AOT works as sodium source and structure-directing agent. This solution was filtered and the precipitate was removed. Then, a mixture of TBOT in ethanol (2.5mmol/15.5 mL) was fast dropped into the filtered solution, and stirred at 80 ºC for 6 h. A white solid product was washed with ethanol and ultrapure water for several times until neutral pH.

For the copper-modified titanium phosphate nanoparticles, an aqueous suspension (1 mL) of TiPNPs (40 mg/mL) was dispersed in 17 mL of an aqueous solution of $Cu(CH_3COO)_2$ (10 mM) and the resulting mixture was stirred at 50 ˚C for 24 h. Then, the final mixture was centrifuged, the solid precipitate was washed three times with 10 mL of ultrapure water and the nanoparticles were dried under vacuum overnight yielding almost quantitatively CuTiPNPs. In order to evaluate the effect of the NaOH solution in the CuTiPNPs structure, 80 mg of CuTiPNPs were dispersed in 5 mL of NaOH solution (0.1 M) and the resulting suspension was stirred for 1 minute. Then, the mixture was centrifuged, the remaining solid was washed three times with ultrapure water and dried under vacuum overnight yielding almost quantitatively CuTiPNPs-OH.

2.4. X-ray photoelectron spectroscopy

Photoelectron spectra were acquired with a Escalab 200R (Vacuum Generators, Ltd., UK) spectrometer provided with a hemispherical electron analyzer and a MgKα1 (*hv* = 1253.6 eV) X-ray source. The spectra were acquired in the constant analyzer energy mode at 200 eV pass energy for survey spectra and 50 eV pass energy for narrow (10-20 eV) scans. The background pressure in the analysis chamber was maintained below 8.10^{-9} mbar during data acquisition. The XPS data signals were taken in increments of 0.07 eV with dwell times of 40 ms. The binding energy scale of the instrument was calibrated with respect to $Au4f_{7/2}$ (84.0 eV) and $Cu2p_{3/2}$ (932.6 eV) emissions. Charge effects on the samples were corrected by taking the C1s line of adventitious carbon at binding energy (BE) of 284.8 eV which gives an accuracy of ± 0.1 eV. Intensities of the peaks were calculated from the respective peak areas after background subtraction and spectrum fitting by the standard computer based statistical analysis which included fitting the experimental spectra to a sum of Gaussian and Lorentzian lines (90G-10L) using a least squares minimization procedure for χ^2 with the help of the *XPS peak* program. Relative surface atomic ratios were determined from the corresponding peak areas, corrected with tabulated sensitivity factors,[38] with a precision of 7%.

2.5. Nanostructuration of the screen-printed electrodes

Modification of 8xSPCEs with CuTiPNPs was carried out by depositing an aliquot of 4 µL of the CuTiPNPs dispersion covering the working electrode surface. The solution was left at room temperature (20°C) until dryness.

2.6. Electrochemical measurements

Glucose detection was carried out by measuring the chronoamperometric response at 60 s after the application of +0.5 V. The value of the current measured at 60 s is considered the analytical signal.

Electrochemical impedance spectroscopy (EIS) was performed with an Autolab PGSTAT12 (Metrohm Autolab) potentiostat/galvanostat controlled by the Autolab FRA 4.9 software. Individual screen-printed carbon electrodes (SPCEs) (DropSens, ref. 110) were used for EIS measurements. 40 µL of $[Fe(CN)_6]^{3-/4-}$ or $[Ru(NH_3)_6]^{2+/3+}$ solution (5 mM) prepared in KCl 0.1 M was dropped on the electrochemical cell and EIS measurements were carried out by applying a potential of +0.12 V (for $[Fe(CN)_6]^{3-/4-}$) or -0.24 V (for $[Ru(NH_3)_6]^{2+/3+}$) and an AC amplitude of 10 mV. The impedance data was fitted to the Randles equivalent circuit (**Figure S2**).

2.7. Real samples

For honey samples, 0.4 g of honey was diluted in 25 mL of H_2O and diluted 100 times in NaOH 0.1 M. 25 µL of this solution was added to the device to carry out the measurement.

For blood, in order to separate the plasma, the sample was centrifuged at 10000 rpm during 3 min. Then, the plasma was diluted 10 times in NaOH 0.1 M. For the standard additions analysis, 500 µL of the diluted plasma was added to 500 µL of a solution of 0, 100, 300 and 700 µM of glucose in NaOH 0.1 M, respectively.

3. RESULTS AND DISCUSSIONS

3.1. Characterization of the copper-modified titanium phosphate nanoparticles

3.1.1. Structural Analysis

Comparing the X-ray diffractogram of CuTiPNPs with that one of the TiPNPs, shown in **Figure S3**, it is easy to see that the incorporation of copper cations to the starting nanoparticles affected not only the amorphous shell but also the crystalline core. In fact, the crystallinity of $NaTi_2(PO_4)_3$, which constitute the core of the nanoparticle, is almost destroyed and probably new phases have been created as far as a new peak appears at $2\theta = 18.1$ and the signal due to the plane (1 1 3) is less intense. These changes could be originated either by a partial incorporation of the copper ions into the crystal structure or by the partial substitution of sodium by copper ions. Actually, NaTi2(PO4)3 is able to incorporate cations into its structure[39–41] or even to exchange sodium by other cations[42,43]. In both cases, it is expected that the crystallinity of the sodium dititanium triphosphate will be altered or even new phases could be formed. The X-ray diffractogram of CuTiPNPs-OH was similar to that of the CuTiPNPs and, therefore, it is not shown.

The IR spectrum of CuTiPNPs does not show any band attributable to the acetate ion (around 1500 cm^{-1}) (**Figure S4**). It means that the acetate ions as well as the acetic acid formed in the reaction between the CH_3COO^- anions and those protons coming from the hydrogen phosphate or dihydrogen phosphate units present in the starting TiPNPs were eliminated when the sample was washed with water. When comparing the whole IR spectrum of CuTiPNPs with that of the starting nanoparticles, the most relevant modifications are located in the 500-700 cm^{-1} region (see **Figure 1**). There are bands at 640 and 581 cm^{-1} that are present in both spectra, although with different intensity. They could be tentatively assigned to $NaTi_2(PO_4)_3$ [44] although the band at 581 cm^{-1}, which is more intense in TiPNPs, could also be attributed to the HO-P=O group[45,46] present in both hydrogenphosphates and dihydrogenphosphates. The lower intensity of the band at 581 cm^{-1} in

the infrared spectrum of CuTiPNPs could be explained taking into account that the copper cations have replaced the protons of the acid phosphates. In the IR spectrum of the copper derivative CuTiPNPs, two new bands at 557 and at 517 cm^{-1} are observed, which should be related to copper phosphates, suggesting that the copper is linked to the phosphate groups of the nanoparticles. In fact, the glass $(CuO)_{0.5}(P_20_5)_{0.5}$ exhibit a PO_4^{3-} band at 523 cm^{-1}[47] and the compound $Cu_3(PO_4)_2$. $2H_2O$ exhibits bands at 633 and 559 cm^{-1} [48]. In order to simulate the behavior of the CuTiPNPs on the electrode surface, the nanoparticles were treated with a 0.1 M NaOH solution (as described previously), generating CuTiPNPs-OH. Some differences are observed in the FTIR spectrum of the sample CuTiPNPs-OH (**Figure 1C**). This spectrum also shows bands at 640 and 555 cm^{-1}, which can be attributed to copper phosphates, suggesting that the copper atoms remain connected to the phosphate groups of the nanoparticles, even after the treatment with the alkaline solution. Furthermore, the disappearance of the band at 581 cm^{-1} (tentatively assigned to HO-P=O) would be explained assuming that the NaOH reacted with most of the protons of the acid phosphates.

3.1.2. Morphological Analysis

The morphology of TiPNPs, CuTiPNPs and CuTiPNPs-OH samples at the nanoscale was studied by transmission electron microscopy (TEM). Representative TEM images of these samples are shown in **Figure 2** and the corresponding particle size distributions are given in **Figure S5**. These distributions and the morphology do not differ so much from each other. It is worth mentioning that no different phases are observed, as it happens for silver-modified TiPNPs, where silver nanoparticles can be observed[29]. This fact suggests that the copper is present within the structure of the CuTiPNPs and it is not forming an alternative species such as other particles, even after treatment with the alkaline solution.

The inter-plane distances of the $NaTi_2(PO_4)_3$ crystals detected by electron diffraction in the TEM experiments, are coincident with those of the same crystal inside the parent TiPNPs:

TiPNPs ---------- CuTiPNPs

4.34 Å-----$NaTi_2(PO_4)_3$ ---- 4.34 Å

3.67 Å----- $NaTi_2(PO_4)_3$ -----3.65 Å

3.00 Å---- $NaTi_2(PO_4)_3$ -----3.03 Å

2.72 Å---- $NaTi_2(PO_4)_3$ -----2.75 Å

Similarly, inter-plane distances of the $NaTi_2(PO_4)_3$ crystals, which constitute the core of CuTiPNPs-OH, detected by electron diffraction in the TEM experiments, are coincident with those of the same crystal inside the parent TiPNPs, although in this case less planes are detected, suggesting greater destruction of this crystalline phosphate, which is in accordance with the disappearance of the band at 580 cm^{-1} in the infrared spectrum of CuTiPNPs-OH (assigned to this compound, $NaTi_2(PO_4)_3$).

3.1.3. Surface Analysis

Photoelectron spectroscopy was used to evaluate the chemical environment of the atoms and to quantify the elemental abundance on the surface region of the solid samples. As the XP survey scan allows identify unambiguously the elements present on solid surfaces, low resolution, wide energy scans were recorded for all the samples. In addition, high-resolution P2p, O 1s, Ti2p, Cu and Na1s spectra were recorded and the corresponding binding energies are summarized in **Table S1**. The binding energy for P2p at 134 eV indicates that phosphorus in the samples exists in pentavalent oxidation state and apparently as P-O bond species[49]. The $Ti2p_{3/2}$ spectrum was satisfactorily fitted as one peak at 458.6 eV indicating that Ti ions are in an octahedral environment, coordinated with oxygen.[50] The Cu2p and O1s spectra of CuTiPNPs and CuTiPNPs-OH samples are displayed in **Figure 3**. The binding energy of the most intense component ($Cu2p_{3/2}$) of the Cu2p doublet in both samples appear at 935.1 and 935.2 eV, respectively, which are characteristic of divalent copper (see **Table S1**). The presence of Cu(II) species is also supported by the typical shake-up observed at ca. 940 and 943 eV. In addition, both CuTiPNPs and CuTiPNPs-OH samples

show the presence of sodium, whose Na1s core level at a binding energy of 1071.4-1071.5 eV is indicative of the presence of Na^+ cations which are required to counterbalance the negative charge of phosphate groups. Quantitative analysis (**Table S2**) revealed that the Cu/Ti atomic ratio is slightly higher for the CuTiPNPs-OH (1.371) sample than for its CuTiPNPs counterpart (1.214) while the Na/Ti ratio follow an opposite trend.

3.2. Electrochemistry of CuTiPNPs-modified screen-printed carbon electrodes

Electrochemical characterization of CuTiPNPs-modified screen-printed electrodes was carried out after the modification of the working electrode with 4 µL of a 2 mg/mL dispersion of CuTiPNPs. A solution of 5 mM of $[Fe(CN)_6]^{4-}$ in KCl 0.1 M was employed as electrochemical indicator. Cyclic voltammograms recorded from +0 V to +0.7 V at several scan rates (10, 25, 50, 100, 250 mV/s) are shown in the **Figure 4**. The characteristic anodic and cathodic processes of the $[Fe(CN)_6]^{3-/4-}$ redox couple can be observed in the voltammograms and the peak current increased linearly with the square root of the scan rate (**Figure S7A**). This fact means that the process is gouverned by the mass transport by semi-infinite linear diffusion, as happens for a bare SPCE electrode (see Supporting Information, **Figures S6** and **S7B**). Therefore, it seems that the porous coating of the electrode surface does not influence the limiting control of the electrochemical reaction. The Randles-Sevcik equation for a one-electron irreversible transfer was employed to estimate the electroactive area of the electrode:

$$\mathbf{i_p = (2.99x10^5)\ \propto^{1/2} A\ C\ D^{1/2}\ v^{1/2}} \qquad \mathbf{(1)}$$

where i_p is the peak current (A), $\propto$ is the electronic transfer coefficient (typically, 0.5), A is the electrode area (cm^2), C is the bulk concentration of the analyte (mol/cm^3), D is the diffusion coefficient of the analyte (0.67×10^{-5} cm^2/s in KCl 0.1 M)[51], and v is the scan rate (V/s). Electroactive area for the CuTiPNPs-modified electrode was 3.4 ± 0.4 mm^2. This area was lower than the estimated area for a bare electrode (4.6 ± 0.5 mm^2). The modification of the electrode

surface with a material such as titanium phosphate has a negative effect on the electrode area that is involved in the electron transfer.

Although some kind of non-metallic nanoparticles could influence directly the electron transfer, as it happens with quantum dots[52,53], it does not seem to be the case for CuTiPNPs since the electrochemical processes are observed at a similar potential to the bare electrode (see S.I., **Table S3**). Therefore, the voltammetric results suggest that the electron transfer is performed directly through the carbon electrode. The lower electroactive area is probably due to that part of the electrode surface is not available because it is blocked by the non-conducting nanoparticles. However, the porous nature of the material and the heterogeneity of the film formed on the electrode surface helps to prevent that the entire electrode surface is hindered for the electron transfer and the decrease on the electroactive area was not as high as expected. This fact is important when the electrodes nanostructured with these nanoparticles are employed for electrocatalytic applications as the electron transfer is possible even with the film coating the working electrode.

In order to get more information on the electron transfer between the electroactive species and the modified electrodes, electrochemical impedance spectroscopy was carried out for bare and CuTiPNPs-modified screen-printed electrodes using a solution of 5 mM of the redox couple $[Fe(CN)_6]^{3-/4-}$ (**Figure 5A**). A significant increment on the charge transfer resistance (R_{ct}) was found for the electrode modified with CuTiPNPs (956 ± 112 Ω) or with TiPNPs (760 ± 95 Ω) compared to the bare electrode (380 ± 52 Ω), as suggests the increment of the semicircle radius. These results clearly show that the electron transfer is hindered by the film of the nanostructured material, fact that was unclear after the voltammetric measurements, causing an increment in the charge transfer resistance. However, it is likely that this lower electron transfer rate is due to the possible repulsion of anions from the pores of the nanoparticles, as the phosphate groups could confer some negative

charge, which prevents access of a negatively-charged redox species, and therefore, inhibit the electron transfer. This possibility was evaluated using the $[Ru(NH_3)_6]^{2+/3+}$ redox couple (positively charged). A R_{ct} of the same order was obtained for bare SPCEs (24 ± 3 Ω) and modified with TiPNPs (30 ± 2 Ω), as illustrated in the **Figure 5B**. Additionally, double-layer capacitances of 1.07 ± 0.02 and 4.4 ± 0.2 µF were estimated for bare and CuTiPNPs-modified electrodes, respectively. The modification of the carbon surface with a film of a mesoporous material, which can be partially charged, increases the capacitance of the electrical double layer. This increment is not due to a higher electroactive area, it may be due to the different dielectric constant of these nanoparticles compared to the dissolution and may also be due to the porous nature and local charge of the nanoparticles, which can influence the reorganization of ions of the double layer, increasing the ability to store electrical charge at the electrode/solution. This electrochemical characterization has provided interesting information about the behaviour of electrodes modified with CuTiPNPs and TiPNPs.

3.3. Non-enzymatic detection of glucose using SPCEs modified with CuTiPNPs

The electrochemical behaviour of bare screen-printed carbon electrodes and modified with 2 mg/mL of CuTiPNPs was studied by linear sweep voltammetry in 0.1 M NaOH in the absence and presence of 1 and 10 mM of glucose (**Figure 4B**). When glucose is present in the solution and the electrodes are modified with CuTiPNPs, an oxidation process can be observed at a potential close to +0.60 V, which increases with the glucose concentration in solution. This process does not occur when bare electrodes are used, indicating a characteristic electrocatalytic process of CuTiPNPs-modified electrodes towards glucose. Although a significant peak response was not appreciable in absence of glucose for the modified electrodes, it was probably due to the low sensitivity of the voltammetric technique for visualizing the direct copper oxidation when no catalytic reaction takes place (and with a small quantity of nanoparticles). However, the increased current of the chronoamperometric response (**Figure S8**) suggests that the oxidation of copper is produced even in

absence of glucose. The voltammetric response obtained is coherent with the glucose oxidation mechanism typically considered for copper-based electrodes in alkaline medium. As previously reported in the literature[54,55], copper (III) oxides and hydroxides could work as a catalyst for the oxidation of sugars (as indicated by the reaction in equations 1,2). In this reaction, glucose is oxidized to gluconolactone by Cu(III), which is generated electrochemically from Cu(II) and Cu(III) is consecutively reduced to regenerate Cu(II). The consumption of Cu(III) in this reaction leads to an increased oxidation process of Cu(II) to Cu(III) (according to Le Chatelier principle), which is directly related to the amount of glucose in solution.

However, as described in the characterization section, the CuTiPNPs, even after a treatment with an alkaline solution, present Cu(II) connected to the phosphate groups of the nanoparticles, and copper oxides or hydroxides were not observed. Therefore, the Cu(II) present in the structure of the CuTiPNPs is the initial species involved in the electrocatalytic reaction. To electrogenerate Cu(III) species at a relatively low potential, as verified experimentally by voltammetry, the Cu(III) should be strongly stabilized in these conditions. Owing to the high reactivity of Cu(III) species and their *in situ* electro-generation only at the electrode surface is really difficult to carry out a structural characterization to know more accurately the mechanism of the formation and the chemical composition of the species involved in the glucose oxidation. However, a possible and reasonable mechanism is proposed. Cu(II) is, probably, bound to the phosphate by oxygen atoms, in a very simplified notation: -P-O-Cu-O-P-. Cu(II) in this species seems to be in a stabilized atmosphere by the strong electronegative oxygen atoms. After the electrooxidation in alkaline medium the following Cu(III) species could be formed (again, in a simplified notation): -P-O-Cu(OH)-O-P. This species is further stabilized by the union of hydroxide groups, which are essential in order to produce the oxidation at a low potential. For CuO electrodes, the mechanism proposed after the electrooxidation is typically by means of CuO(OH), in an analogous process to the proposed for the CuTiPNPs in our work (**Figure 6**). Another possibility is that the electrooxidation of Cu(II) species

were capable of extracting the metal from the CuTiPNPs structure to generate oxides/hydroxides on the electrode surface. However, this mechanism would involve a major reorganization of bonds (breaking copper-phosphate bonds and generating new oxide/hydroxide bonds), which theoretically would have slower kinetics that the previous proposed mechanism and that would result in a shift of the oxidation potential to more positive potentials (higher energy). In the voltammetric measurements, the Cu(II) to Cu(III) oxidation appears to a potential close to +0.6 V, which is very similar to the potential found for the oxidation of CuO described in different published studies[17,56]. In these cases, with the electrooxidation of Cu(II) to Cu(III) only a new bound is generated to obtain CuO(OH). Therefore, the energy (potential) necessary to oxidize the Cu(II) of the CuTiPNPs is similar to CuO, suggesting that a similar mechanism takes place. This mechanism would indicate the formation of Cu(III) species stabilized by phosphate groups and hydroxide ions, interesting aspect due to that Cu(III) species have only been reported under complex conditions[23,57].

In order to obtain more information on the electrochemical process, a study of the catalytic oxidation of glucose at the nanostructured device was carried out. Linear-sweep voltammograms of a solution of 10 mM glucose in 0.1 M NaOH at several scan rates from 10 to 250 mV/s were recorded (shown in **Figure S9A**). A linear relationship between the oxidation peak current versus the square root of the scan rate was found (**Figure S9B**), suggesting that the limiting step for the rate of the electrochemical reaction is the diffusion of species to the electrode surface. This fact is coherent with the results found by other authors[58]. Although the copper species on the electrode surface are decisive for the reaction (Cu(II) to Cu(III)), other species such as the glucose or the OH^- ions are also involved, and the results suggest that the mass transport of some of these species control the limiting step of the reaction, and they do not interact strongly with the electrode surface or with the CuTiPNPs.

3.3.1. Optimization of the experimental conditions

The performance of electrochemical device using CuTiPNPs and 8xSPCEs for the oxidation of glucose was optimized by varying different experimental conditions such as the amount of CuTiPNPs deposited on the electrode surface or the effect of the applied potential. The results are described in the Supporting Information (**S10**).

3.3.2. Analytical performance of the electrochemical device

In order to evaluate the analytical characteristics of the developed device for glucose determination, increasing concentrations of glucose in 0.1 M NaOH were measured with different devices using the optimized experimental conditions. The chronoamperometric response showed a linear relationship to the glucose concentration from 25 µM to 2 mM (**Figure 7A**) with a correlation coefficient (R^2) of 0.997 according to the following equation: i (µA) = 0.401 (± 0.009) [Glucose](mM) + 0.023 (± 0.006) (n=3). A detection limit of 7 µM of glucose was obtained. The detection limit was calculated as the concentration corresponding to three times the standard deviation of the estimate[59]. The electrochemical device developed using screen-printed electrodes modified with CuTiPNPs exhibited excellent performance for glucose with a wide linear range, a sensitivity of 7.81 µA mM^{-1} cm^{-2} and a low detection limit. The detection limit of the developed device is much smaller than the normal values found in most samples of interest (clinical or food samples), so the device could be used for glucose detection in these samples.

Several copper and nickel-based screen-printed electrodes for non-enzymatic glucose determination are presented in **Table 1**. Although other metal-based electrodes have been reported in the literature (specially based on noble metals), the trend is to use cheaper materials such as copper and nickel, and small, low-cost and disposable devices such as screen-printed electrodes. Two of the electrodes reported seem more competitive considering the analytical characteristics obtained. For instance, the work published by Liang-Sung *et al.*[60], in which the help of graphene produces a very

sensitive device with an extremely low limit of detection. However, the analytical characteristics are calculated using the device in a flow-injection analysis setup, which typically improves the limit of detection. The electrode modified with 3D nickel nanoporous structures also shows a good performance[61]. This device is employed in a conventional electrochemical cell with stirring, enhancing the mass transport and therefore, the limit of detection. In comparison to the other screen-printed devices reported, our device is highly competitive in terms of the linear range and limit of detection. Moreover, the utilization of 8-channel screen-printed cards leads to the simultaneous determination of 8 glucose samples, resulting in a considerable time-effective analysis.

3.3.3. Precision and stability studies

A precision study of the electrochemical device was carried out by evaluating the reproducibility of eight different electrodes modified with CuTiPNPs using the optimized conditions and tested with a solution of 300 µM of glucose in 0.1 M NaOH. The developed device showed precise results with an average relative standard deviation (RSD) of 8.5%.

The stability of the electrochemical device was evaluated, several screen-printed electrodes were modified with CuTiPNPs using the optimized conditions and stored at run temperature for different time periods. The chronoamperometric response of the devices was tested by triplicate over a 6-week period using a solution of 200 µM of glucose in 0.1 M NaOH. As shown in **Figure 7B**, the device kept the initial response for the time period tested, verifying the good stability. This fact is due to the good stability of the titanium phosphate nanoparticles after the introduction of Cu(II), allowing the deposited film on the electrode surface to keep their initial conditions.

3.3.4. Interference study of the electrochemical device

In order to evaluate the selectivity of the electrochemical device towards glucose oxidation, several possible interfering species such as dopamine, uric acid, ascorbic acid and other sugars were tested. Studies are described in the Supporting Information (**Figure S11**). In summary, the device exhibit excellent selectivity towards glucose.

3.3.5. Real samples

In order to evaluate the performance of the electrochemical device developed in this work for real samples, the determination of glucose in food and clinical samples was carried out. A honey sample was diluted as explained previously, obtaining a solution with a glucose concentration within the calibration range. The sample was measured by triplicate and the value of the current intensity was used with the calibration curve to obtain a glucose concentration of 29 ± 3 g/100g sample. This value is very close to the value obtained (29.3 ± 0.4 / 100g sample) with another device previously developed in our group that was validated for different samples[62]. Therefore, the device showed a good performance towards glucose detection in a sample with a high concentration of other sugars such as fructose, and, therefore, showing a negligible response to these species. Furthermore, no significant matrix effects were observed with the dilution performed (1:100).

Glucose determination in a blood clinical sample was performed by following the procedure described in the Experimental section. A scheme of this procedure is shown in the **Figure S12**. The results were validated with a commercial glucometer (One Touch Ultra Easy, LifeScan). In order to avoid problems with the high concentration of proteins, samples were centrifuged at 10000 rpm for 3 min to perform the separation of the plasma. As the typical glucose concentration in blood is significantly higher than the calibration range of the device, a dilution of the plasma was carried out (1:10) in 0.1 M NaOH. This solution was measured with the electrochemical device under the optimized conditions and the chronoamperometric current was used to obtain a concentration value from the calibration plot (Figure 7A). However, the results for this sample were well below the real

value obtained by the commercial glucometer, suggesting a high impact of matrix issues. Then, a standard addition method (**Figure S13**) was carried out to minimize these issues, getting a value closer to the value obtained by the glucometer (100 ± 11 mg dL^{-1} vs. 104 ± 5 mg dL^{-1} with the glucometer). Although the aqueous portion is separated and the appropriate dilution made in NaOH, matrix interferences seems to occur. However, the analysis by the standard additions method appears to be suitable for using this non-enzymatic electrochemical device with complex samples.

4. CONCLUSIONS

This work describes, for the first time, the modification of titanium phosphate nanoparticles with copper and the direct electrocatalysis towards the oxidation of glucose. The characterization studies have provided more insight on the structural, morphological and electrochemical properties of the TiPNPs modified with metals. Cu(II) seems to be bound to the nanoparticles by the phosphate groups. Furthermore, no structural or morphological changes were observed after treatment with an alkaline solution. Therefore, a mechanism of the glucose electrocatalysis is proposed where electrogenerated Cu(III) species stabilized by the phosphate groups of the nanoparticles are involved, different from the typical CuO species reported in the literature. Furthermore, CuTiPNPs were used in 8-channel screen-printed cards for non-enzymatic glucose determination, obtaining a good analytical performance, the detection of glucose at µM concentrations, and the ability to perform eight simultaneous analyses, quickly and easily. This work could open a new way to develop electrocatalytic application using titanium phosphate nanoparticles modified with different metals, which could allow the catalysis of other electrochemical reactions of interest.

SUPPORTING INFORMATION

Additional text, ten figures, and three tables showing the multichannel electrodes, spectra data, several electrochemical experiments, optimization of the experimental conditions and interference study for the glucose detection.

ACKNOWLEDGEMENTS

This work has been supported by the FC-15-GRUPIN-021 project from the Asturias Regional Government and the CTQ2014-58826-R project from the Spanish Ministry of Economy and Competitiveness (MEC). Daniel Martín-Yerga thanks the MEC for the award of a FPI grant (BES-2012-054408).

NOTES

The authors declare no competing financial interest.

REFERENCES

[1] E. Costa Rama, J. Biscay, M.B. González García, a Julio Reviejo, J.M. Pingarrón Carrazón, A. Costa-García, Comparative study of different alcohol sensors based on Screen-Printed Carbon Electrodes., Anal. Chim. Acta. 728 (2012) 69–76. doi:10.1016/j.aca.2012.03.039.

[2] J. Biscay, E. Costa Rama, M.B. González García, A. Julio Reviejo, J.M. Pingarrón Carrazón, A.C. García, Amperometric fructose sensor based on ferrocyanide modified screen-printed carbon electrode., Talanta. 88 (2012) 432–8. doi:10.1016/j.talanta.2011.11.013.

[3] L. Wang, E. Wang, A novel hydrogen peroxide sensor based on horseradish peroxidase immobilized on colloidal Au modified ITO electrode, Electrochem. Commun. 6 (2004) 225–229. doi:10.1016/j.elecom.2003.12.004.

[4] J. Wang, Electrochemical glucose biosensors., Chem. Rev. 108 (2008) 814–25. doi:10.1021/cr068123a.

[5] N.S. Oliver, C. Toumazou, a. E.G. Cass, D.G. Johnston, Glucose sensors: A review of current and emerging technology, Diabet. Med. 26 (2009) 197–210. doi:10.1111/j.1464-5491.2008.02642.x.

[6] J. Ju, J. Bai, X. Bo, L. Guo, Non-enzymatic acetylcholine sensor based on Ni-Al layered double hydroxides/ordered mesoporous carbon, Electrochim. Acta. 78 (2012) 569–575. doi:10.1016/j.electacta.2012.06.051.

[7] N. Jia, B. Huang, L. Chen, L. Tan, S. Yao, A simple non-enzymatic hydrogen peroxide sensor using gold nanoparticles-graphene-chitosan modified electrode, Sens. Actuators B. 195 (2014) 165–170. doi:10.1016/j.snb.2014.01.043.

[8] S. Park, H. Boo, T.D. Chung, Electrochemical non-enzymatic glucose sensors., Anal. Chim. Acta. 556 (2006) 46–57. doi:10.1016/j.aca.2005.05.080.

[9] K. Toghill, R. Compton, Electrochemical non-enzymatic glucose sensors: a perspective and an evaluation, Int. J. Electrochem. Sci. 5 (2010) 1246–1301.

[10] G. Wang, X. He, L. Wang, A. Gu, Y. Huang, B. Fang, B. Geng, X. Zhang, Non-enzymatic electrochemical sensing of glucose, Microchim. Acta. 180 (2012) 161–186. doi:10.1007/s00604-012-0923-1.

[11] D.E. Pissinis, L.E. Sereno, J.M. Marioli, Non-enzymatic sensing of carbohydrates using a nickel-chromium alloy electrode, Sens. Actuators B. (2013). doi:10.1016/j.snb.2013.10.122.

[12] H. Tian, M. Jia, M. Zhang, J. Hu, Nonenzymatic glucose sensor based on nickel ion implanted-modified indium tin oxide electrode, Electrochim. Acta. (2013). doi:10.1016/j.electacta.2013.02.096.

[13] F. Wang, S. Hu, Electrochemical sensors based on metal and semiconductor nanoparticles, Microchim. Acta. 165 (2009) 1–22. doi:10.1007/s00604-009-0136-4.

[14] P. Si, Y. Huang, T. Wang, J. Ma, Nanomaterials for electrochemical non-enzymatic glucose biosensors, RSC Adv. 3 (2013) 3487. doi:10.1039/c2ra22360k.

[15] H. Wang, C. Fan, Copper oxide nanostructures: Controlled synthesis and their catalytic performance, Solid State Sci. 16 (2013) 130–133. doi:10.1016/j.solidstatesciences.2012.11.009.

[16] P. Samarasekara, N.T.R.N. Kumara, N.U.S. Yapa, Sputtered copper oxide (CuO) thin films for gas sensor devices, J. Phys. Condens. Matter. 18 (2006) 2417–2420. doi:10.1088/0953-8984/18/8/007.

[17] Q. Chen, L. Zhang, G. Chen, Facile Preparation of Graphene-Copper Nanoparticle Composite by in Situ Chemical Reduction for Electrochemical Sensing of Carbohydrates, Anal. Chem. 84 (2012) 171–178. doi:10.1021/ac2022772.

[18] S. V Prabhu, R.P. Baldwin, Constant potential amperometric detection of carbohydrates at a copper-based chemically modified electrode, Anal. Chem. 61 (1989) 852–856. doi:10.1021/ac00183a014.

[19] Y. Tian, Y. Liu, W. Wang, X. Zhang, W. Peng, CuO nanoparticles on sulfur-doped graphene for nonenzymatic glucose sensing, Electrochim. Acta. 156 (2015) 244–251. doi:10.1016/j.electacta.2015.01.016.

[20] J.M. Marioli, T. Kuwana, Electrochemical characterization of carbohydrate oxidation at copper electrodes, Electrochim. Acta. 37 (1992) 1187–1197. doi:10.1016/0013-4686(92)85055-P.

[21] M.Z. Luo, R.P. Baldwin, Characterization of carbohydrate oxidation at copper electrodes, J. Electroanal. Chem. 387 (1995) 87–94. doi:10.1016/0022-0728(95)03867-G.

[22] J.P. Fox, B. Ramdhanie, A.A. Zareba, R.S. Czernuszewicz, D.P. Goldberg, Copper(III) and Vanadium(IV)-Oxo Corrolazines, Inorg. Chem. 43 (2004) 6600–6608. doi:10.1021/ic049384a.

[23] F.C. Anson, T.J. Collins, T.G. Richmond, B.D. Santarsiero, J.E. Toth, B.G.R.T. Treco, Highly stabilized copper(III) complexes, J. Am. Chem. Soc. 109 (1987) 2974–2979. doi:10.1021/ja00244a020.

[24] J. Liu, X. Wei, Y. Yu, J. Song, X. Wang, A. Li, X.-W. Liu, W.-Q. Deng, Uniform core-shell titanium phosphate nanospheres with orderly open nanopores: a highly active Brønsted acid catalyst., Chem. Commun. (Camb). 46 (2010) 1670–2. doi:10.1039/b922100j.

[25] K. Jia, B. Pan, L. Lv, Q. Zhang, X. Wang, B. Pan, W. Zhang, Impregnating titanium phosphate nanoparticles onto a porous cation exchanger for enhanced lead removal from waters., J. Colloid Interface Sci. 331 (2009) 453–7. doi:10.1016/j.jcis.2008.11.068.

[26] L.-N. Feng, J. Peng, Y.-D. Zhu, L.-P. Jiang, J.-J. Zhu, Synthesis of Cd(2+)-functionalized titanium phosphate nanoparticles and application as labels for electrochemical immunoassays., Chem. Commun. (Camb). 48 (2012) 4474–6. doi:10.1039/c2cc31552a.

[27] L.-N. Feng, Z.-P. Bian, J. Peng, F. Jiang, G.-H. Yang, Y.-D. Zhu, D. Yang, L.-P. Jiang, J.-J. Zhu, Ultrasensitive multianalyte electrochemical immunoassay based on metal ion functionalized titanium phosphate nanospheres., Anal. Chem. 84 (2012) 7810–5. doi:10.1021/ac301438v.

[28] F. Cheng, T. He, H. Miao, J. Shi, L. Jiang, J. Zhu, Electron Transfer Mediated Electrochemical Biosensor for MicroRNAs Detection Based on Metal Ion Functionalized Titanium Phosphate Nanospheres at Attomole Level, ACS Appl. Mater. Interfaces. 7 (2015) 2979–2985. doi:10.1021/am508690x.

[29] D. Martín-Yerga, J. Carrasco-Rodríguez, M.B. González-García, F.J. García Alonso, A. Costa-García, Determination of Silver-Modified Titanium Phosphate Nanoparticles by Voltammetric and Electrocatalytic Methods, Electroanalysis. 26 (2014) 2574–2579. doi:10.1002/elan.201400519.

[30] M. Maltez-da Costa, A. de la Escosura-Muñiz, C. Nogués, L. Barrios, E. Ibáñez, A. Merkoçi, Detection of circulating cancer cells using electrocatalytic gold nanoparticles., Small. 8 (2012) 3605–12. doi:10.1002/smll.201201205.

[31] S. Zuo, Y. Teng, H. Yuan, M. Lan, Direct electrochemistry of glucose oxidase on screen-printed electrodes through one-step enzyme immobilization process with silica sol-gel/polyvinyl alcohol hybrid film, Sensors Actuators, B Chem. 133 (2008) 555–560. doi:10.1016/j.snb.2008.03.024.

[32] J. Liu, S. Sun, C. Liu, S. Wei, An amperometric glucose biosensor based on a screen-printed electrode and Os-complex mediator for flow injection analysis, Measurement. 44 (2011) 1878–1883. doi:10.1016/j.measurement.2011.09.001.

[33] H.-C. Liu, C.-C. Tsai, G.-J. Wang, Glucose biosensors based on a gold nanodendrite modified screen-printed electrode., Nanotechnology. 24 (2013) 215101. doi:10.1088/0957-4484/24/21/215101.

[34] D. Martín-Yerga, M.B. González-García, A. Costa-García, Electrochemical immunosensor for anti-tissue transglutaminase antibodies based on the in situ detection of quantum dots., Talanta. 130 (2014) 598–602. doi:10.1016/j.talanta.2014.07.010.

[35] D. Martín-Yerga, A. Costa-García, Towards a blocking-free electrochemical immunosensing strategy for anti-transglutaminase antibodies using screen-printed electrodes., Bioelectrochemistry. 105 (2015) 88–94. doi:10.1016/j.bioelechem.2015.05.014.

[36] J. Biscay, M.B.G. García, A.C. García, Electrochemical biotin determination based on a screen printed carbon electrode array and magnetic beads, Sens. Actuators B. 205 (2014) 426–432. doi:10.1016/j.snb.2014.08.042.

[37] M.M.P.S. Neves, M.B. González-García, D. Hernández-Santos, P. Fanjul-Bolado, Screen-Printed Electrochemical 96-Well Plate : a High- Throughput Platform for Multiple Analytical Applications, Electroanalysis. 26 (2014) 2764–2772. doi:10.1002/elan.201400388.

[38] C.D. Wagner, L.E. Davis, M. V. Zeller, J.A. Taylor, R.H. Raymond, L.H. Gale, Empirical atomic sensitivity factors for quantitative analysis by electron spectroscopy for chemical analysis, Surf. Interface Anal. 3 (1981) 211–225. doi:10.1002/sia.740030506.

[39] L. Chen, L. Zhang, X. Zhou, Z. Liu, Aqueous Batteries Based on Mixed Monovalence Metal Ions: A New Battery Family, ChemSusChem. 7 (2014) 2295–2302. doi:10.1002/cssc.201402084.

[40] S. Patoux, C. Masquelier, Lithium Insertion into Titanium Phosphates, Silicates, and Sulfates, Chem. Mater. 14 (2002) 5057–5068. doi:10.1021/cm0201798.

[41] S. Il Park, I. Gocheva, S. Okada, J. Yamaki, Electrochemical Properties of NaTi2(PO4)3 Anode for Rechargeable Aqueous Sodium-Ion Batteries, J. Electrochem. Soc. 158 (2011) A1067. doi:10.1149/1.3611434.

[42] N. Hirose, J. Kuwano, Ion-exchange properties of NASICON-type phosphates with the frameworks [Ti2(PO4)3] and [Ti1.7Al0.3(PO4)3], J. Mater. Chem. 4 (1994) 9. doi:10.1039/jm9940400009.

[43] A. Tsuji, H. Takahashi, T. Oi, Preparation of ion exchangers in the hydrogen form from M1+xTi2P3–xSixO12 (M = Li, Na) crystals and glass-ceramics and their characterization, J. Mater. Chem. 13 (2003) 542–549. doi:10.1039/b207611j.

[44] V.I. Pet'kov, E. a. Asabina, a. V. Markin, N.N. Smirnova, Synthesis, characterization and thermodynamic data of compounds with NZP structure, J. Therm. Anal. Calorim. 91 (2008) 155–161. doi:10.1007/s10973-007-8370-7.

[45] K. Rajendran, C. Dale Keefe, Growth and characterization of calcium hydrogen phosphate dihydrate crystals from single diffusion gel technique, Cryst. Res. Technol. 45 (2010) 939–945. doi:10.1002/crat.200900700.

[46] J. Xu, D. F.R. Gilson, I. S. Butler, FT-Raman and high-pressure FT-infrared spectroscopic investigation of monocalcium phosphate monohydrate, Ca(H2PO4)2·H2O, Spectrochim. Acta Part A Mol. Biomol. Spectrosc. 54 (1998) 1869–1878. doi:10.1016/S1386-1425(98)00152-8.

[47] M. a. Salim, G.D. Khattak, M.S. Hussain, X-ray photoelectron spectroscopy, fourier transform infrared spectroscopy and electrical conductivity studies of copper phosphate glasses, J. Non. Cryst. Solids. 185 (1995) 101–108. doi:10.1016/0022-3093(94)00683-0.

[48] X. Wu, G. Shi, Fabrication of a lotus-like micro-nanoscale binary structured surface and wettability modulation from superhydrophilic to superhydrophobic, Nanotechnology. 16 (2005) 2056–2060. doi:10.1088/0957-4484/16/10/013.

[49] S.J. Splinter, R. Rofagha, N.S. McIntyre, U. Erb, XPS Characterization of the Corrosion Films Formed on Nanocrystalline Ni-P Alloys in Sulphuric Acid, Surf. Interface Anal. 24 (1996) 181–186. doi:10.1002/(SICI)1096-9918(199603)24:3<181::AID-SIA92>3.0.CO;2-N.

[50] D. Zhao, C. Chen, Y. Wang, H. Ji, W. Ma, L. Zang, J. Zhao, Surface Modification of TiO2 by Phosphate: Effect on Photocatalytic Activity and Mechanism Implication, J. Phys. Chem. C. 112 (2008) 5993–6001. doi:10.1021/jp712049c.

[51] S.J. Konopka, B. McDuffie, Diffusion coefficients of ferri- and ferrocyanide ions in aqueous media, using twin-

electrode thin-layer electrochemistry, Anal. Chem. 42 (1970) 1741–1746. doi:10.1021/ac50160a042.

[52] C. Stoll, S. Kudera, W.J. Parak, F. Lisdat, Quantum dots on gold: Electrodes for photoswitchable cytochrome c electrochemistry, Small. 2 (2006) 741–743. doi:10.1002/smll.200500441.

[53] D. Martín-Yerga, E.C. Rama, A. Costa-García, Electrochemical Study and Applications of Selective Electrodeposition of Silver on Quantum Dots, Anal. Chem. 88 (2016) 3739–3746. doi:10.1021/acs.analchem.5b04568.

[54] X. Kang, Z. Mai, X. Zou, P. Cai, J. Mo, A sensitive nonenzymatic glucose sensor in alkaline media with a copper nanocluster/multiwall carbon nanotube-modified glassy carbon electrode, Anal. Biochem. 363 (2007) 143–150.

[55] L.C. Jiang, W. De Zhang, A highly sensitive nonenzymatic glucose sensor based on CuO nanoparticles-modified carbon nanotube electrode, Biosens. Bioelectron. 25 (2010) 1402–1407. doi:10.1016/j.bios.2009.10.038.

[56] N. a. Choudhry, D.K. Kampouris, R.O. Kadara, N. Jenkinson, C.E. Banks, Next generation screen printed electrochemical platforms: Non-enzymatic sensing of carbohydrates using copper(ii) oxide screen printed electrodes, Anal. Methods. 1 (2009) 183. doi:10.1039/b9ay00095j.

[57] P.J. Donoghue, J. Tehranchi, C.J. Cramer, R. Sarangi, E.I. Solomon, W.B. Tolman, Rapid C-H bond activation by a monocopper(III)-hydroxide complex, J. Am. Chem. Soc. 133 (2011) 17602–17605. doi:10.1021/ja207882h.

[58] S. Felix, P. Kollu, B.P.C. Raghupathy, S.K. Jeong, A.N. Grace, Electrocatalytic oxidation of carbohydrates and dopamine in alkaline and neutral medium using CuO nanoplatelets, J. Electroanal. Chem. 739 (2015) 1–9. doi:10.1016/j.jelechem.2014.12.006.

[59] J.N. Miller, J.C. Miller, Statistics and Chemometrics for Analytical Chemistry, Pearson Education Limited, Essex, England, 2010.

[60] C.-L. Sun, W.-L. Cheng, T.-K. Hsu, C.-W. Chang, J.-L. Chang, J.-M. Zen, Ultrasensitive and highly stable nonenzymatic glucose sensor by a CuO/graphene-modified screen-printed carbon electrode integrated with flow-injection analysis, Electrochem. Commun. 30 (2013) 91–94. doi:10.1016/j.elecom.2013.02.015.

[61] X. Niu, M. Lan, H. Zhao, C. Chen, Highly sensitive and selective nonenzymatic detection of glucose using three-dimensional porous nickel nanostructures., Anal. Chem. 85 (2013) 3561–9. doi:10.1021/ac3030976.

[62] J. Biscay, E. Costa Rama, M.B. González García, J.M. Pingarrón Carrazón, A. Costa-García, Enzymatic Sensor Using Mediator-Screen-Printed Carbon Electrodes, Electroanalysis. 23 (2011) 209–214. doi:10.1002/elan.201000471.

[63] T.K. Huang, K.W. Lin, S.P. Tung, T.M. Cheng, I.C. Chang, Y.Z. Hsieh, C.Y. Lee, H.T. Chiu, Glucose sensing by electrochemically grown copper nanobelt electrode, J. Electroanal. Chem. 636 (2009) 123–127. doi:10.1016/j.jelechem.2009.08.011.

[64] M. García, A. Escarpa, A class-selective and reliable electrochemical monosaccharide index in honeys, as determined using nickel and nickel-copper nanowires., Anal. Bioanal. Chem. 402 (2012) 945–53. doi:10.1007/s00216-011-5453-x.

[65] M. García, A. Escarpa, Disposable electrochemical detectors based on nickel nanowires for carbohydrate sensing., Biosens. Bioelectron. 26 (2011) 2527–33. doi:10.1016/j.bios.2010.10.049.

[66] C.-H. Lien, J.-C. Chen, C.-C. Hu, D.S.-H. Wong, Cathodic deposition of binary nickel-cobalt hydroxide for non-enzymatic glucose sensing, J. Taiwan Inst. Chem. Eng. 45 (2014) 846–851. doi:10.1016/j.jtice.2013.09.023.

[67] M. Hjiri, R. Dhahri, N. Ben Mansour, L. El Mir, M. Bonyani, A. Mirzaei, S.G. Leonardi, G. Neri, Electrochemical properties of a novel Ni-doped nanoporous carbon, Mater. Lett. 160 (2015) 452–455. doi:10.1016/j.matlet.2015.08.001.

[68] J. Yang, J.-H. Yu, J. Rudi Strickler, W.-J. Chang, S. Gunasekaran, Nickel nanoparticle–chitosan-reduced graphene oxide-modified screen-printed electrodes for enzyme-free glucose sensing in portable microfluidic devices, Biosens. Bioelectron. 47 (2013) 530–538. doi:10.1016/j.bios.2013.03.051.

Figure 1

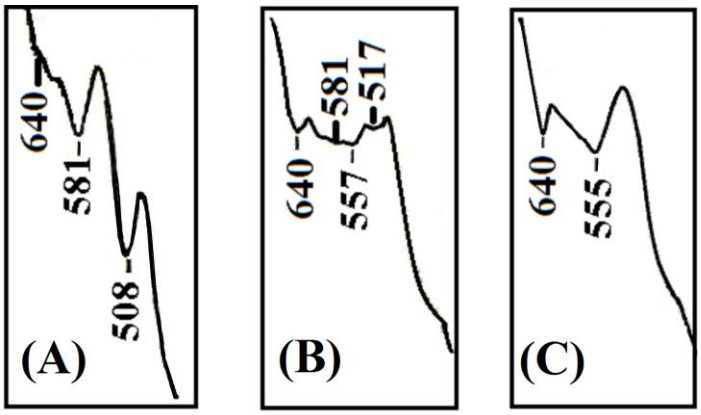

Figure 1. IR spectra in the 500-700 cm^{-1} range for A) TiPNPs, B) CuTiPNPs and C) CuTiPNPs-OH.

Figure 2

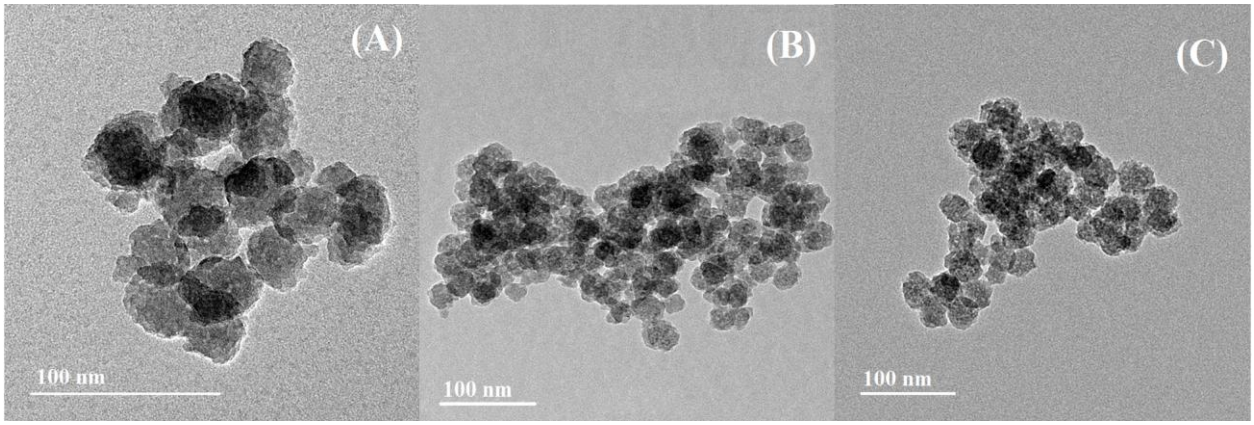

Figure 2. Representative TEM images for A) TiPNPs, B) CuTiPNPs and C) CuTiPNPs-OH.

Figure 3

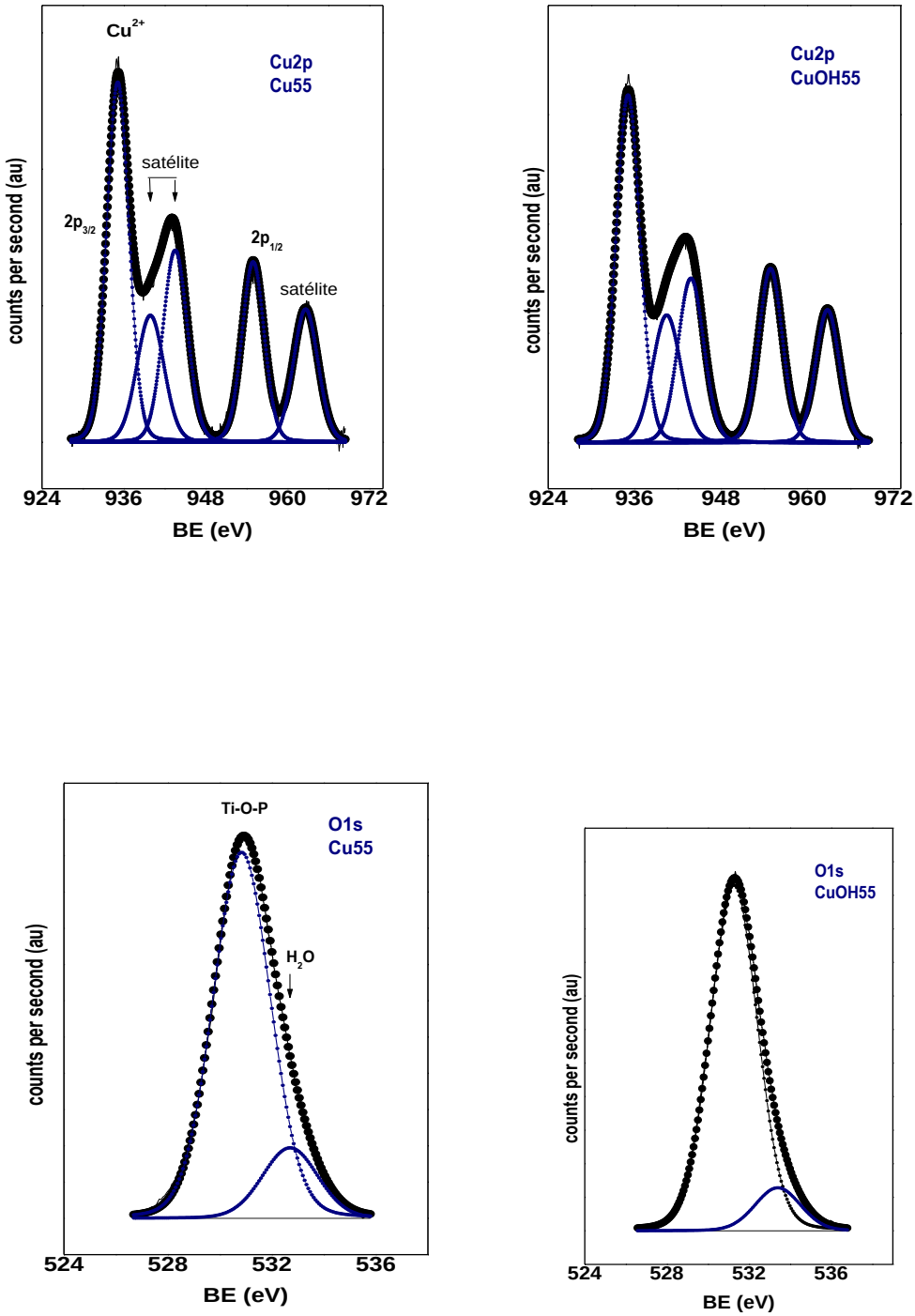

Figure 3. Cu2p and O1s XPS spectra for CuTiPNPs and CuTiPNPs-OH.

Figure 4

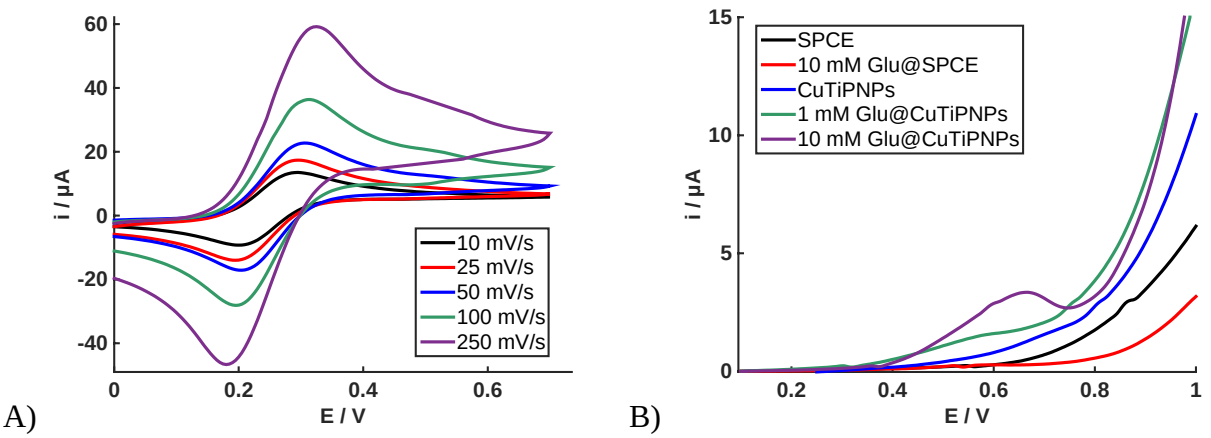

Figure 4. **A)** Voltammetric response for ferrocyanide using CuTiPNPs-modified electrodes at different scan rates (10, 25, 50, 100, 250 mV/s). **B)** Linear-sweep voltammograms in 0.1 M NaOH for bare and CuTiPNPs-modified electrodes in presence or absence of 1 or 10 mM of glucose.

Figure 5

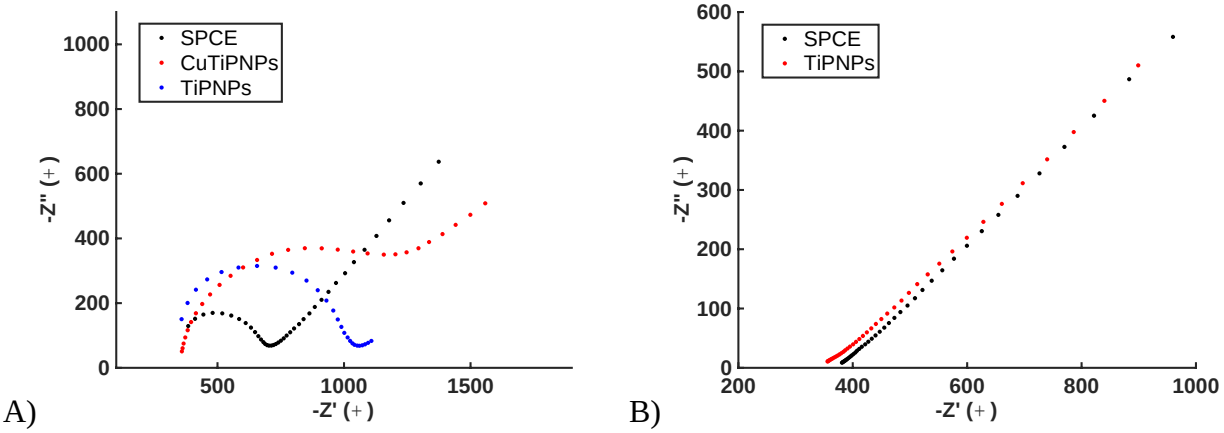

Figure 5. **A)** Nyquist plots for bare, TiPNPs and CuTiPNPs-modified electrodes using the $[Fe(CN)_6]^{3-/4-}$ couple redox. **B)** Nyquist plots for bare and TiPNPs-modified electrodes using the $[Ru(NH_3)_6]^{2+/3+}$ couple redox.

Figure 6

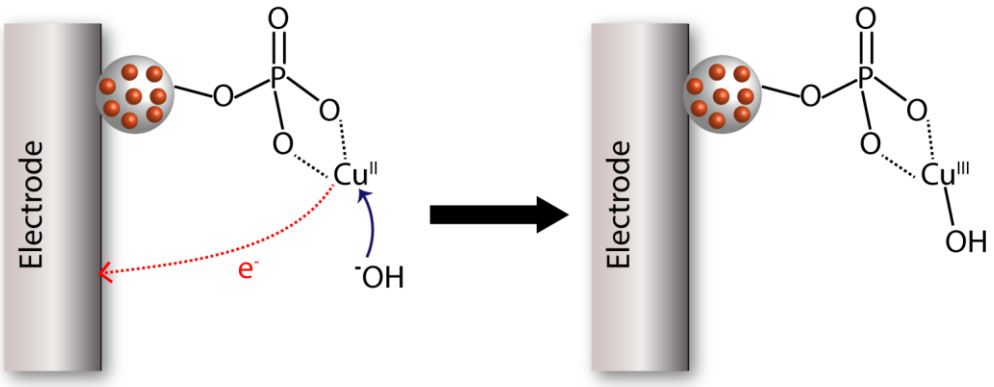

Figure 6. Schematic mechanism proposed for the formation of the Cu(III) species after the electrooxidation.

Figure 7

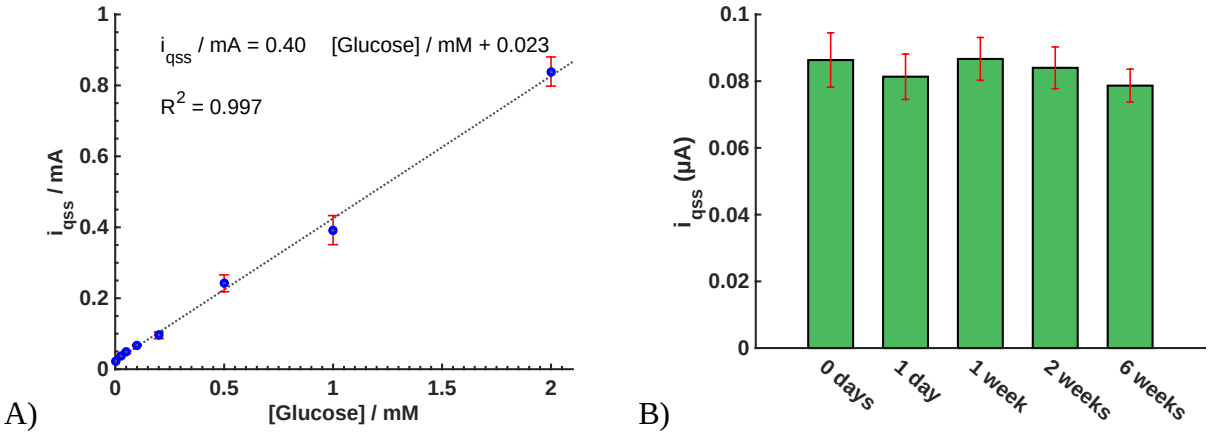

Figure 7. A) Calibration plot representing the relationship between the quasi-stationary current and the glucose concentration. **B)** Chronoamperometric quasi-stationary current obtained in several CuTiPNPs-modified electrodes stored at ambient conditions for different periods of time.

Table 1

Electrode material	Linear Range (µM)	Detection Limit (µM)	Reference
CuTiPNPs	**25-2000**	**7**	**This work**
Cu nanobelt	10 – 1130	10	[63]
Cu/Graphene	0.12 – 500	0.03	[60]
CuOSPEs	50 - 1200	4	[56]
NiCu nanowires	50-1000	40	[64]
Ni nanowires	50-1000	-	[65]
NiCo	25-3700	-	[66]
Ni-doped nanoporous carbon	20-240	10	[67]
3D-porous Ni nanostructures	0.5-4000	0.07	[61]
NiNP-chitosan-rGO	200-9000	4.1	[68]

Table 1. Analytical characteristics of several non-enzymatic glucose devices using screen-printed electrodes.

SUPPORTING INFORMATION

Copper-modified titanium phosphate nanoparticles as electrocatalyst for glucose detection

*Daniel Martín-Yerga[1], Javier Carrasco-Rodríguez[2], José Luis G. Fierro[3], Francisco Javier García Alonso[2] and Agustín Costa-García[1]**

[1]Departamento de Química Física y Analítica, Universidad de Oviedo, Oviedo, Spain

[2]Departamento de Química Orgánica e Inorgánica, Universidad de Oviedo, Oviedo, Spain

[3]Instituto de Catálisis y Petroleoquímica, CSIC, Cantoblanco, 28049 Madrid, Spain

*E-mail: costa@uniovi.es

Contents

S1. Multichannel screen-printed electrodes

The electrodes used throughout the work were 8-channel screen-printed cards (purchased from DropSens). A schematic diagram is shown in **Figure S1A** and a real image is shown in **Figure S1B**. These cards are composed by eight miniaturized electrochemical cells with a carbon working electrode of 2.56 mm in diameter. Electrochemical cells are independent and different electrochemical methods can be applied simultaneously. Using a multichannel potentiostat (DropSens µStat 8000), we were able to perform 8 simultaneous analyses, resulting in a time-effective research in comparison to use individual screen-printed electrodes or conventional electrodes.

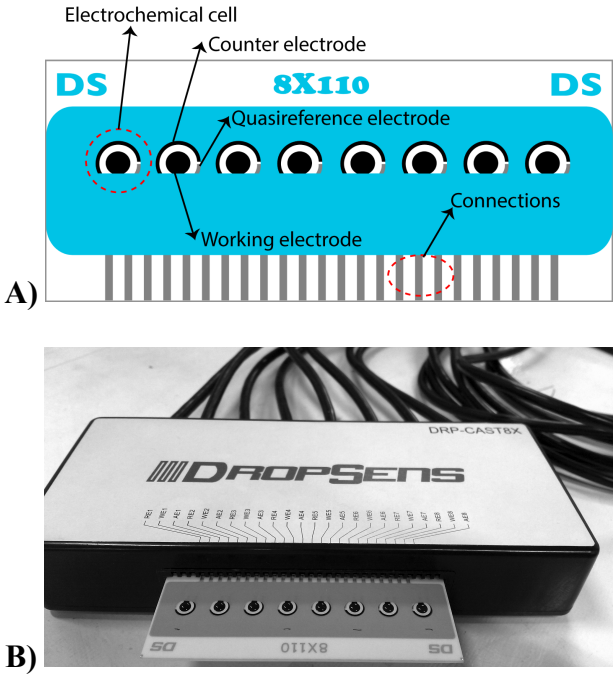

Figure S1. **A)** Schematic diagram and **B)** image of the 8-channel electrochemical screen-printed electrodes.

S2. Equivalent circuit employed for the impedimetric measurements

The equivalent circuit used to fit the impedimetric response for the different cases was the Randles circuit (**Figure S2**). This circuit is composed by the solution resistance (Rs), charge transfer resistance (Rct), capacitance of the double layer (Cdl) and Warburg diffusion element (W). Its is interesting to mention that this circuit was enough to successfully fit the response, and it was not necessary to add

other elements that would affect the impedimetric response, such as the effect of the porous semiconductor materials, which is coating the electrode surface.

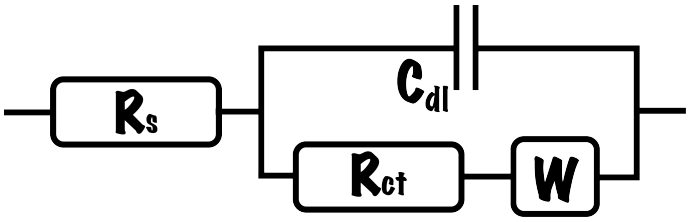

Figure S2. Randles equivalent circuit employed for fitting the impedimetric responses.

S3. X-Ray Diffraction spectra

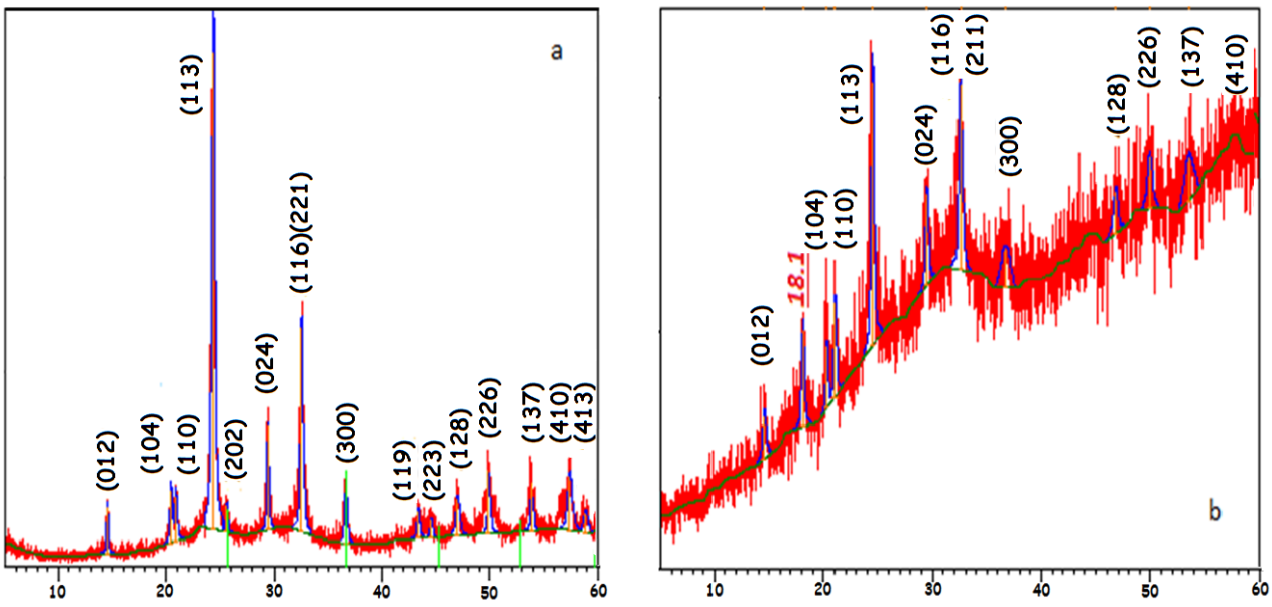

Figure S3. X-Ray diffractograms for a) TiPNPs (coincident with JCPDS No. 33-1296, see also reference [1]) and b) CuTiPNPs.

S4. Infrared spectra of the titanium phosphate nanoparticles

The complete infrared spectra for TiPNPs, CuTiPNPs and CuTiPNPs-OH are shown in the **Figure S4**.

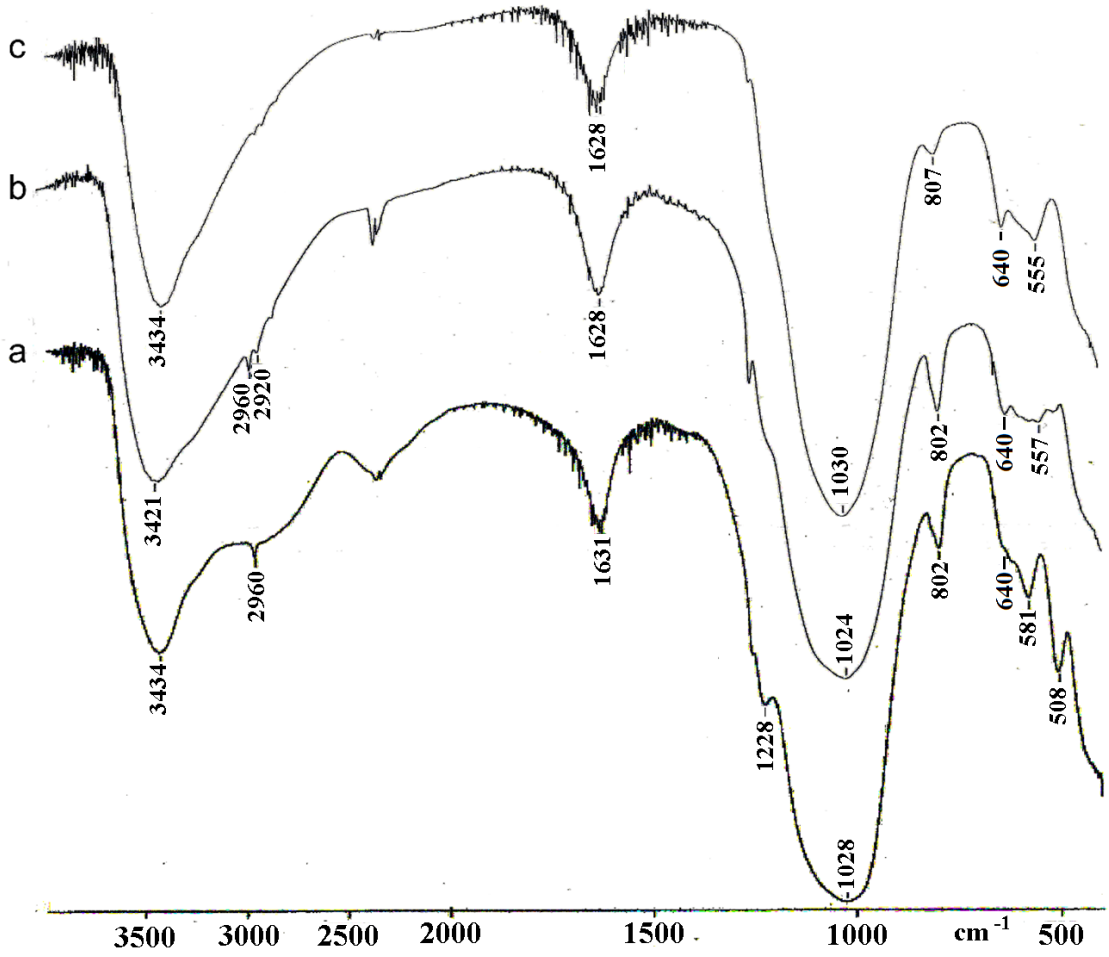

Figure S4. Complete IR spectra obtained for TiPNPs, CuTiPNPs and CuTiPNPs-OH.

S5. Size distributions estimated by Transmission electron microscopy

The size distribution of the nanoparticles (**Figure S5**) was estimated by analyzing the micrographs obtained by transmission electron microscopy of the different syntthesized products (TiPNPs, CuTiPNPs and CuTiPNPs-OH). The average size for the nanoparticles was 30±5 nm, 31±5 nm and 28±5 nm, respectively.

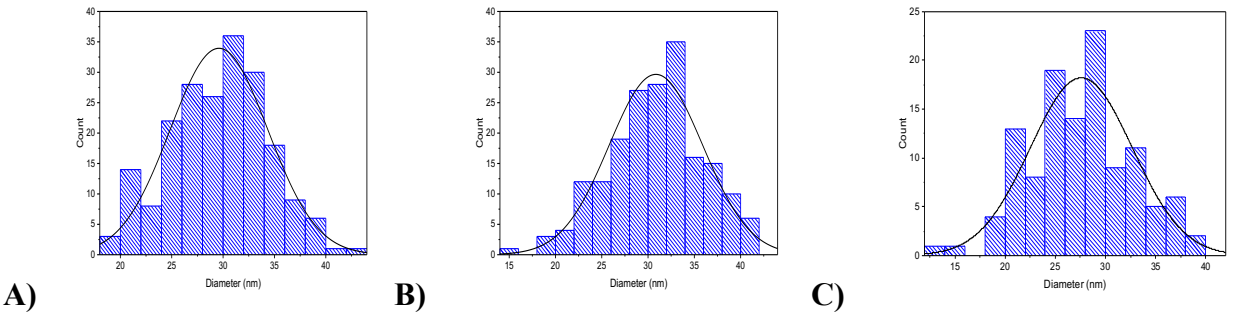

Figure S5. Size distributions estimated by transmission electron microscopy of **A)** TiPNPs, **B)** CuTiPNPs and **C)** CuTiPNPs-OH.

S6. Binding energies of the X-ray Photoelectron Spectroscopy measurements

Table S1. Binding energies of the peaks obtained in the XPS spectra for TiPNPs, CuTiPNPs and CuTiPNPs-OH. The value of the ratio between the areas of the satellite line and main peak for Cu2p3/2 is shown in red color. The O1s peak shows two components: the most intense (84-89%) is assigned to O^{2-} of the structure and the peak with lower intensity (11-16%) is assigned to adsorbed molecular water.

	Cu2p3/2	P2p	Ti2p3/2	O1s	Na1s
TiPNPs		133.6	459.6	531.3 (84) 533.0 (16)	1071.5
CuTiPNPs	935.1 (0.729)	133.4	459.5	530.8 (87) 532.7 (13)	1071.4
CuTiPNPs-OH	935.2 (0.714)	133.6	459.5	531.3 (89) 533.3 (11)	1071.5

Table S2. Surface atomic ratios obtained from the XPS data fot TiPNPs, CuTiPNPs and CuTiPNPs-OH.

	Cu/Ti	P/Ti	Na/Ti
TiPNPs	-	4.170	0.493
CuTiPNPs	1.214	2.412	0.268
CuTiPNPs-OH	1.371	1.933	0.149

S7. Electrochemical behavior of ferrocyanide at bare and modified electrodes

The electrochemical behavior of a model redox species such as ferrocyanide was studied using bare and CuTiPNPs-modified screen-printed carbon electrodes. **Figure S6** shows the voltammetric response obtained for 5 mM of $[Fe(CN)_6]^{4-}$ in 0.1 M KCl after applying a cyclic sweep from 0 to +0.7 V at different scan rates (10, 25, 50, 100 and 250 mV/s). An anodic and cathodic process can be observed, which can be asigned to the oxidation of $[Fe(CN)_6]^{4-}$ to $[Fe(CN)_6]^{3-}$ and the correspondent reduction. **Figure 4A** in the main manuscript shows the voltammetric response obtained in the same experimental conditions using CuTiPNPs-modified electrodes. The behavior obtained was very similar in both cases, so the modification with CuTiPNPs did not appear to significantly affect the electrochemical reaction. However, the variation of the anodic peak current with the scan rate was studied in order to understand if the modification with the porous semiconductor nanomaterial could affect the mass transfer to the electrode. The anodic peak current was plotted in function of the square root of the scan rate (**Figure S7**). For an electrochemical reaction limited by the diffusion of the species to the electrode surface, this variation should be linear according to the Randles-Sevcik equation (equation 1 in the main manuscript). As shown in **Figure S7**, for bare and modified electrodes, the peak current was proportional to the square root of the scan rate, suggesting that the electrochemical reaction behaves similarly in both cases.

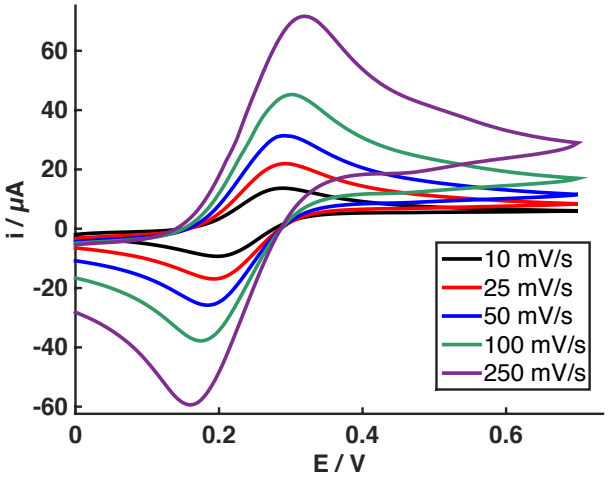

Figure S6. Cyclic voltammetry of ferrocyanide at different scan rates (10, 25, 50, 100 and 250 mV/s) using bare screen-printed carbon electrodes.

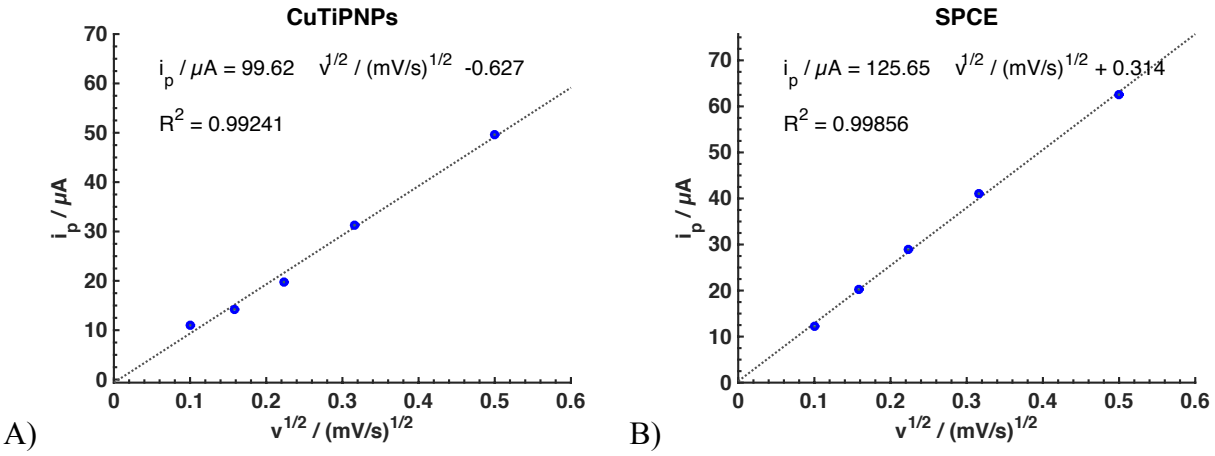

Figure S7. **A)** Relationship of the peak current with the square root of the scan rate for CuTiPNPs-modified electrodes. **B)** Relationship of the peak current with the square root of the scan rate for bare screen-printed electrodes.

Additionally, the potential at which the anodic and cathodic peaks appear, the difference between the peak potentials, and its variation with the scan rate, could provide qualitative information on the kinetics of the electrochemical reaction. Values for these parameters obtained for bare and CuTiPNPs-modified electrodes are shown in the **Table S2**. These data show that the difference in the peak

potentials at bare and modified electrodes is very narrow. Therefore, the voltammetric data obtained with the ferrocyanide species does not show any effect of the modification with CuTiPNPs to the electron transfer or the mass transfer in this reaction. The peak potential difference is similar and increased with the scan rate for both cases, indicative of an irreversible process. For these reasons, the electrochemical impedance spectroscopy measurements were very interesting in order to understand the effect of these nanoparticles in the electron transfer, as explained in the manuscript.

Tabla S3. Voltammetric data (anodic peak potential (Epa), cathodic peak potential (Epc) and peak potential difference (ΔEp)) obtained at bare and CuTiPNPs-modified screen-printed electrode using ferrocyanide at different scan rates (v).

v (mV/s)	SPCE			CuTiPNPs		
	Epa (mV)	Epc (mV)	ΔEp (mV)	Epa (mV)	Epc (mV)	ΔEp (mV)
10	290±3	200±2	90	295±2	200±1	95
25	292±2	194±3	98	297±1	194±1	103
50	291±3	184±4	107	309±4	197±3	112
100	302±1	176±3	126	321±2	188±2	133
500	317±2	170±1	147	333±3	176±2	157

S8. Chronoamperometric response for bare and modified electrodes in absence of glucose

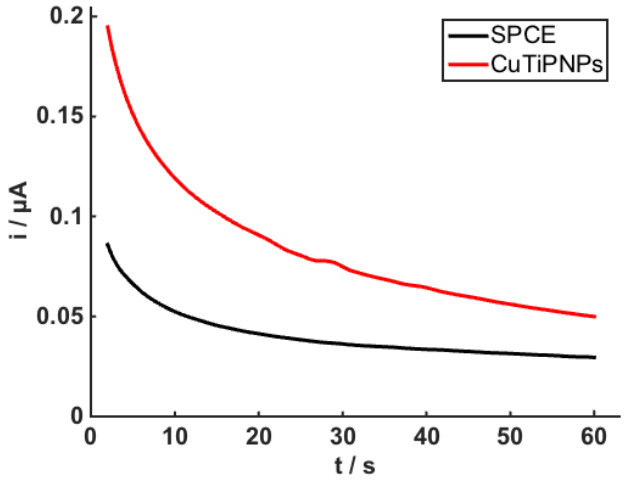

Figura S8. Chronoamperometric response at +0.6 V for a NaOH 0.1 M solution using bare screen-printed electrodes (black curve) and electrodes modified with 2 mg/mL of CuTiPNPs (red curve). A higher quasi-stationary current is obtained for the modified electrodes due to the Cu(II) oxidation at these potentials.

S9. Influence of the scan rate in the electrocatalytic response

Figure S9A shows the voltammetric response obtained at different scan rates (10, 25, 50, 100 mV/s) in a solution of 10 mM of glucose (0.1 M NaOH) using CuTiPNPs-modified electrodes. **Figure S9B** shows the variation of the peak current with the square root of the scan rate. This relationship is linear, suggesting that the catalytic process of the glucose oxidation is limited by the diffusion of species to the electrode surface. As in the electrocatalytic reaction, both glucose and OH^- ions in the solution are involved, it is unclear which of the two species is the limiting one, or even if both could have a significant effect.

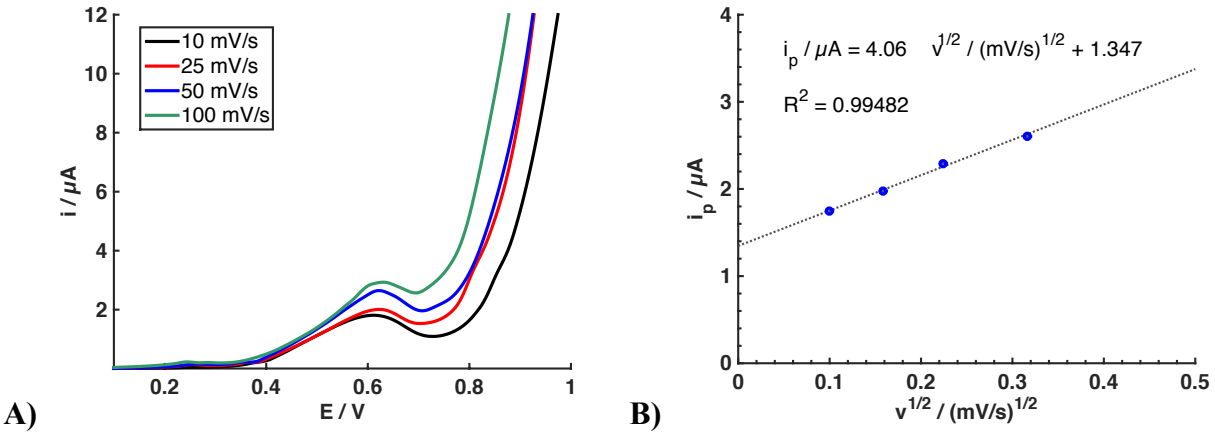

Figure S9. A) Linear-sweep voltammograms for 10 mM of glucose at different scan rates (10, 25, 50 and 100 mV/s). **B)** Relationship between the peak current and the square root of the scan rate.

S10. Optimization of the experimental conditions for the glucose detection

The performance of electrochemical device using CuTiPNPs and 8xSPCEs for the oxidation of glucose was optimized by varying different experimental conditions such as the amount of CuTiPNPs deposited on the electrode surface or the effect of the applied potential. The results are described in the Supporting Information. 0.1 M NaOH was chosen as the electrolytic medium as it is the standard medium for the non-enzymatic detection of glucose using copper or nickel-based nanomaterials.

The effect of the amount of CuTiPNPs deposited on the electrode surface was examined. Several SPCEs were modified with 4 µL of a CuTiPNPs dispersion in H_2O with different concentrations (1, 2, 5, 7, 10 and 20 mg mL^{-1}). Chronoamperometry was performed by applying a potential of +0.6 V for 60 s. As shown in **Figure S10A**, a variation of the analytical signal for the background (0.1 M NaOH) and for a solution containing 1 mM of glucose was found. The ratio between the current obtained for the glucose solution and the background reaches a maximum for a concentration of 5 mg mL^{-1} of CuTiPNPs. At higher concentrations, the ratio decreases, probably due to the difficulty to generate a homogenous film on the electrode surface under these conditions.

The effect of the applied potential (+0.3, +0.4, +0.5, +0.6 V) on the signal/background ratio using a 0.5 mM solution of glucose was also evaluated. The analytical signal increased until a potential of

+0.5 V, remaining rather constant at more positive potentials, while that the background signal increased using more positive potentials (**Figure S10B**). Therefore, +0.5 V was selected as the most suitable potential for the glucose determination.

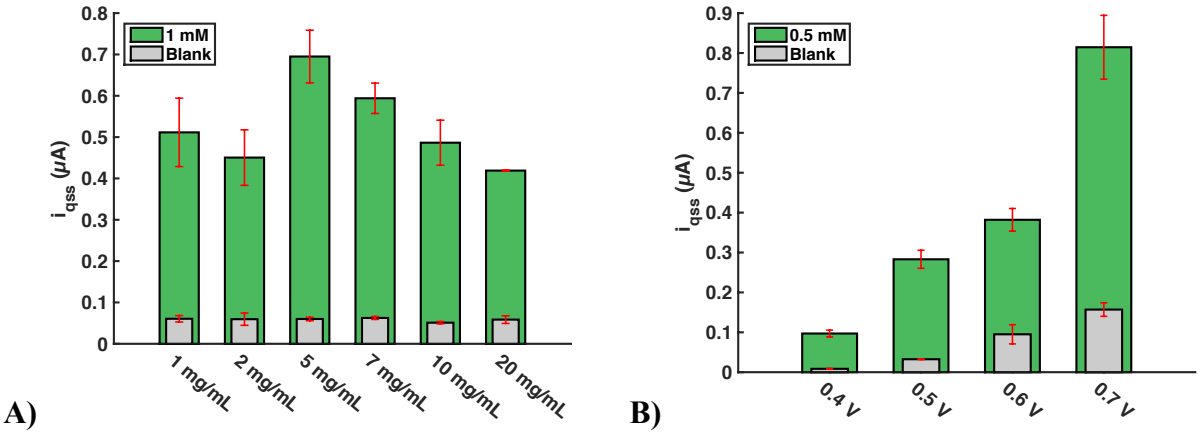

Figure S10. **A)** Effect of the CuTiPNPs concentration on the chronoamperometric quasi-stationary current for 1 mM of glucose (green) and blank solution (grey). **B)** Effect of the applied potential on the chronoamperometric quasi-stationary current for 0.5 mM of glucose (green) and blank solution (grey).

S11. Interference study of the electrochemical device

In order to evaluate the selectivity of the electrochemical device towards glucose oxidation, several possible interfering species were tested. For instance, some electroactive species possibly coexisting in clinical samples such as dopamine, uric acid and ascorbic acid were measured with the device on the same conditions as for glucose using a 0.1 mM concentration of the interfering species in 0.1 M NaOH. Considering that in human serum the glucose concentration is at least 30 times higher than the concentration of AA, UA and DA[2], a solution of 1 mM (only 10 times higher) of glucose was used for comparison. A minor response was observed for DA and UA compared to the background signal (**Figure S11A**). However, the chronoamperometric signal for 1 mM glucose was significantly higher than the signal obtained for these species. Therefore, the device exhibit excellent selectivity towards glucose in clinical samples. Furthermore, in order to evaluate the selectivity of the device for food

control, the response towards different sugars such as fructose, sucrose and xylose was studied. The signal obtained for 100 µM of each sugar compared to the same concentration for glucose is shown in **Figure S11B**. The device produced a minor response towards xylose and fructose, but significantly lower than for glucose detection. Therefore, it can be concluded that the non-enzymatic electrochemical device has a good selectivity for glucose over other sugars, as have been reported for other copper-based electrodes[2].

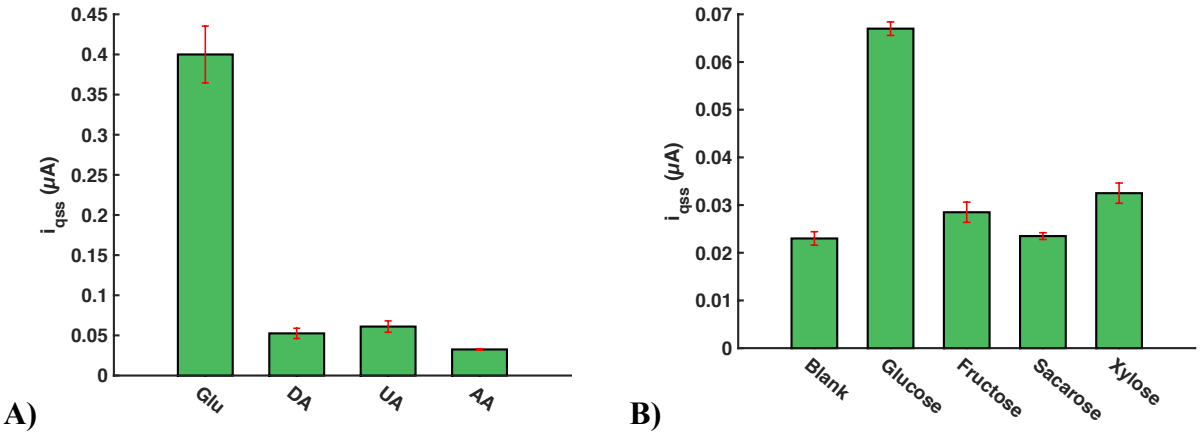

Figure S11. **A)** Chronoamperometric quasi-stationary current obtained for 1 mM of glucose (Glu), 0.1 mM of dopamine (DA), 0.1 mM of uric acid (UA) or 0.1 mM of ascorbic acid (AA). **B)** Chronoamperometric quasi-stationary current obtained for 0.1 mM of several sugars and a blank solution.

S12. <u>Determination of glucose in blood samples</u>

Firstly, as was described in the main manuscript, glucose determination was peformed on blood samples after an initial pretreatment with the aim of separating the protein material and with the appropriate dilution to obtain a response within the calibration linear range (0.025 - 2 mM). A scheme of this pretreatment is shown at the top of the **Figure S12**. The resulting solution was measured by chronoamperometry under the optimized conditions and the obtained current was employed for obtaining the concentration value from the calibration plot (**Figure 7A** of the main manuscript). The result obtained was 67±6 mg/dL, which was well below the value obtained with a commercial glucometer (91±7 mg/dL). Therefore, the determination of glucose was performed by the standard

additions method (**Figure S13**) using the diluted plasma solution after performing the pretreatment of the blood (**Figure S12**). Under these conditions, the results obtained agreed with those obtained by the commercial glucometer (results described in the main manuscript), suggesting that some matrix issues could be present in the direct determination.

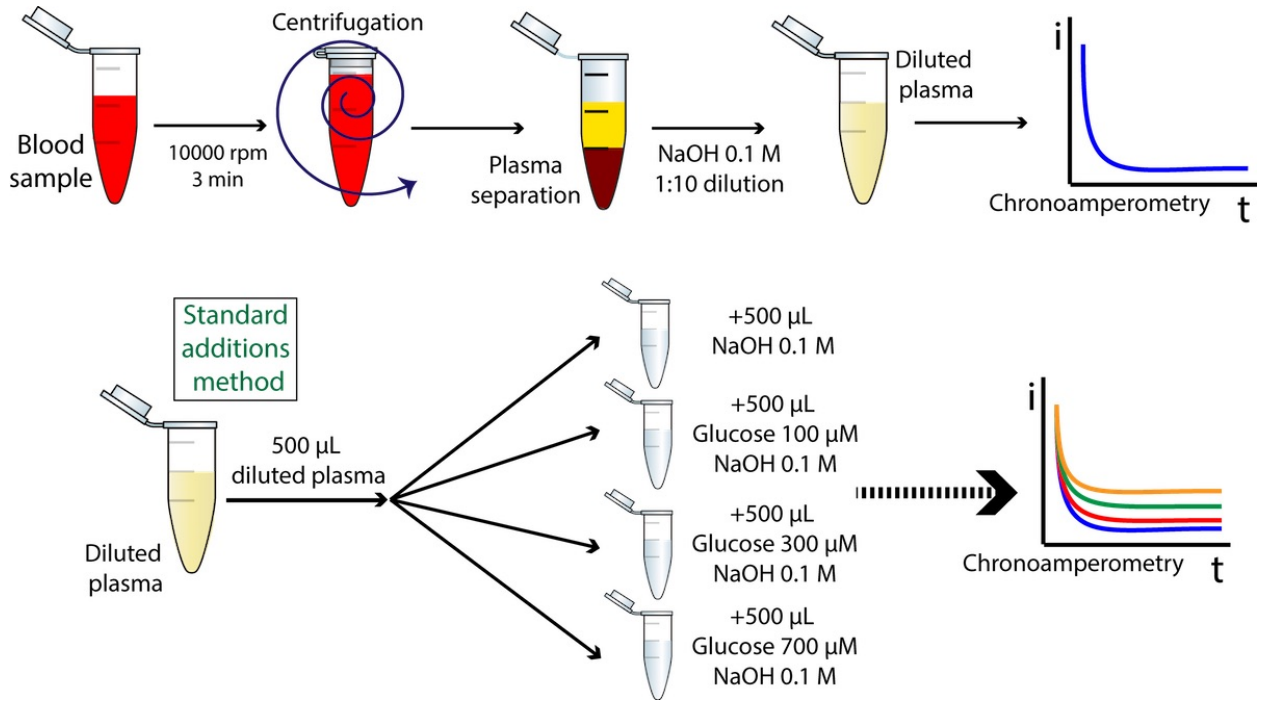

Figure S12. Scheme of the procedure for the blood sample preparation and the standard additions method.

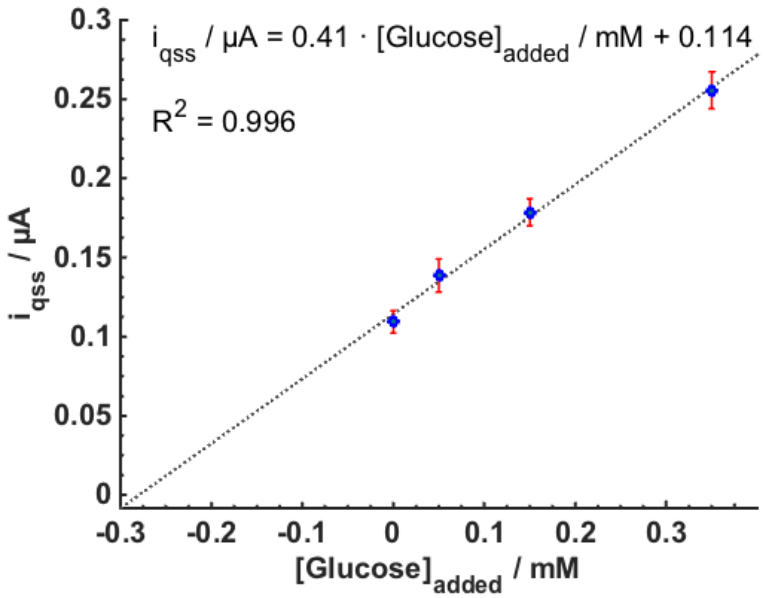

Figure S13. Standard additions plot for the determination of glucose in a blood sample.

References

[1] H. Güler, F. Kurtuluş, A rapid synthesis of sodium titanium phosphate, NaTi2(PO4)3 by using microwave energy, Mater. Chem. Phys. 99 (2006) 394–397. doi:10.1016/j.matchemphys.2005.11.011.

[2] Z. Zhuang, X. Su, H. Yuan, Q. Sun, D. Xiao, M.M.F. Choi, An improved sensitivity non-enzymatic glucose sensor based on a CuO nanowire modified Cu electrode., Analyst. 133 (2008) 126–132. doi:10.1039/b712970j.